

Neural Optimal Transport in Hilbert Spaces: Characterizing Spurious Solutions and Gaussian Smoothing

Jae-Hwan Choi¹ Jiwoo Yoon² Dohyun Kwon^{*3 1} Jaewoong Choi^{*2}

Abstract

We study Neural Optimal Transport in infinite-dimensional Hilbert spaces. In non-regular settings, Semi-dual Neural OT often generates spurious solutions that fail to accurately capture target distributions. We analytically characterize this spurious solution problem using the framework of regular measures, which generalize Lebesgue absolute continuity in finite dimensions. To resolve ill-posedness, we extend the semi-dual framework via a Gaussian smoothing strategy based on Brownian motion. Our primary theoretical contribution proves that under a regular source measure, the formulation is well-posed and recovers a unique Monge map. Furthermore, we establish a sharp characterization for the regularity of smoothed measures, proving that the success of smoothing depends strictly on the kernel of the covariance operator. Empirical results on synthetic functional data and time-series datasets demonstrate that our approach effectively suppresses spurious solutions and outperforms existing baselines.

1. Introduction

Optimal transport (OT) has established itself as a central framework for constructing correspondences between distributions (Villani et al., 2009; Santambrogio, 2015). To scale OT to modern high-dimensional learning pipelines, recent “Neural OT” approaches parameterize OT objects—such as potentials, maps, and couplings—using neural networks (Fan et al., 2023; Choi et al., 2025; Rout et al., 2022). However, in many emerging applications, the underlying data are more naturally modeled as *functions* or *paths*—for example, solutions to PDEs, or time series, or random fields

^{*}Equal contribution ¹Korea Institute for Advanced Study, Seoul, Republic of Korea ²Department of Statistics, Sungkyunkwan University, Seoul, Republic of Korea ³Department of Mathematics, University of Seoul, Seoul, Republic of Korea. Correspondence to: Jaewoong Choi <jaewoongchoi@skku.edu>, Dohyun Kwon <dh.dohyun.kwon@gmail.com>.

Preprint. February 17, 2026.

(Kovachki et al., 2023; Wang et al., 2025; Li et al., 2020). This shift necessitates an OT formulation on an infinite-dimensional Hilbert space H , rather than on the Euclidean space \mathbb{R}^d .

The classical OT theory on general Polish spaces provides foundational results regarding the existence of optimal plans (e.g. (Santambrogio, 2015; Ambrosio et al., 2005)). On the other hand, the existence and uniqueness of the *Monge map* T^* , which is essential for the neural parameterization of a transport map, are not guaranteed in this general setting.

In the Euclidean space \mathbb{R}^d , the concept of absolute continuity with respect to the Lebesgue measure is a sufficient condition for the existence and uniqueness of the Monge map (Brenier, 1991; Gangbo & McCann, 1996). Since real-world data often lie on lower-dimensional manifolds—violating this condition—smoothing strategies, such as adding Gaussian noise to the source measure (Choi et al., 2025), have been proposed to restore well-posedness. However, since there is no infinite-dimensional analogue of the Lebesgue measure, this concept cannot be directly extended to a Hilbert space setting.

Neural Optimal Transport in Hilbert Spaces In light of these obstacles, this work presents an analytical framework for Semi-dual Neural Optimal Transport in Hilbert spaces H . In this framework, the transport map T_θ and potential V_ϕ are parameterized via the following max-min formulation:

$$\sup_{V_\phi \in S_c} \inf_{T_\theta: \mathcal{X} \rightarrow \mathcal{Y}} \mathcal{L}(V_\phi, T_\theta) \quad \text{where} \quad \mathcal{L}(V, T) := \int_{\mathcal{X}} (c(x, T(x)) - V(T(x))) \mu(dx) + \int_{\mathcal{Y}} V(y) \nu(dy). \quad (1)$$

This formulation is known to suffer from the *spurious solution problem* (Rout et al., 2022; Fan et al., 2023; Choi et al., 2025; Chu et al., 2026). An optimal solution to the max-min objective does not necessarily recover the true optimal transport map T^* . Let a pair (V^*, T_{rec}) as an optimal max-min solution if

$$V^* \in \arg \max_{V \in S_c} \inf_{T: \mathcal{X} \rightarrow \mathcal{Y}} \mathcal{L}(V, T), \quad (2)$$

$$T_{\text{rec}} \in \arg \min_{T: \mathcal{X} \rightarrow \mathcal{Y}} \mathcal{L}(V^*, T). \quad (3)$$

It is well-known that the true pair of Kantrovich potential and optimal transport map (V^*, T^*) constitutes an optimal max-min solution. However, not every optimal solution recovers the true transport map, meaning T_{rec} may differ significantly from T^* (see also Examples in Section G.1).

This subtlety arises when the inner minimization problem admits multiple global minimizers, potentially leading to the selection of an invalid map. To eliminate such spurious solutions, we must ensure that the optimal map is uniquely characterized by the potential:

$$\{T^*(x)\} = \arg \min_{y \in H} [c(x, y) - V^*(y)] \quad (4)$$

is uniquely determined μ -almost everywhere. In the finite-dimensional Euclidean setting, Choi et al. (2025) has established that it is ensured if the source measure μ does not assign mass to sets with Hausdorff dimension at most $d - 1$.

In Theorem 3.2, we obtain the relationship (Eq. 4) of the Monge map in an infinite-dimensional Hilbert space H under the *regular* condition on the source measure μ , which serves as a natural generalization of absolute continuity. Moreover, we establish the consistency of the SNOT framework in this regular setting. Specifically, we prove that if μ is regular, and (V^*, T^*) is an optimal max-min solution, then T^* is the Monge map when V^* is a Kantorovich potential.

Ill-posedness and Gaussian Smoothing. Despite the theoretical guarantees established for regular measures, practical data in infinite-dimensional Hilbert spaces often lie on low-dimensional manifolds, violating the regular condition. This setting has been studied for functional data in various contexts. See (Wang et al., 2016) and references therein. In such non-regular settings, the consistency result (Theorem 3.2) is no longer valid. Consequently, the max-min formulation (Eq. 1) becomes severely ill-posed, suffering from the spurious solution problem previously discussed.

To overcome this, we propose a regularization strategy based on *Gaussian smoothing*. We construct a perturbed source variable by adding independent Gaussian noise: $\mathbf{X}^\gamma := \mathbf{X} + \mathbf{G}$, where \mathbf{X} represents the source data (supported on a low-dimensional manifold), and \mathbf{G} is a Hilbert-space valued Gaussian random vector equation (19).

We provide a theoretical characterization (Theorem 4.3) establishing that the smoothing ensures the regular condition if and only if the projection of the source distribution onto the *kernel* of the covariance operator of \mathbf{G} is regular. Practically, this implies that the noise must be injected along the singular directions of the data manifold. Furthermore, we prove that this regularization is consistent: as the smoothing vanishes (by decaying $\lambda_k \rightarrow 0$), the sequence of unique optimal maps T_k^* generates plans that converge weakly to a true optimal plan π^* of the original problem (Theorem

4.2). This validates Gaussian smoothing not merely as a heuristic, but as a theoretically sound method to recover optimal couplings in infinite-dimensional spaces.

Our contributions can be summarized as follows:

- (Theorem 3.2) We prove that, under regular assumptions on the source measure, the semi-dual OT method yields a unique optimal transport map.
- (Theorem 4.3 & Theorem 4.2) We propose a regularization strategy based on Gaussian smoothing, which ensures the regular condition.
- (Section 5) We empirically verify our theoretical findings and evaluate the practical utility of our model (HiSNOT) by achieving state-of-the-art performance on real-world high-dimensional time-series imputation benchmarks.

2. Background

Optimal Transport The Optimal Transport (OT) problem is a mathematical framework that investigates the transport problem between the source measure μ and the target measure ν (Villani et al., 2009; Santambrogio, 2015). Formulated by Monge (1781), the Monge OT problem defines the optimal transport map as a deterministic measurable function T that minimizes the total transport cost:

$$\mathcal{T}(\mu, \nu) := \inf_{T \# \mu = \nu} \left[\int_{\mathcal{X}} c(x, T(x)) \mu(dx) \right]. \quad (5)$$

The pushforward constraint $T \# \mu = \nu$ ensures that the map T transforms the distribution μ into ν , i.e., if $x \sim \mu$, then $T(x) \sim \nu$. Despite its intuitive nature, the Monge problem is inherently non-convex, and the existence of an optimal transport map generally requires regularity assumptions on the measures μ and ν as well as on the cost function c .

To address these limitations, Kantorovich (1948) proposed a convex relaxation of the Monge problem by allowing mass splitting via joint probability measures. The Kantorovich problem is defined as:

$$C(\mu, \nu) := \inf_{\pi \in \Pi(\mu, \nu)} \left[\int_{\mathcal{X} \times \mathcal{Y}} c(x, y) \pi(dx, dy) \right], \quad (6)$$

We refer to the joint probability distribution $\pi \in \Pi(\mu, \nu)$ as the *transport plan* between μ and ν . Unlike the Monge OT problem, the optimal transport plan (OT Plan) π^* is guaranteed to exist under mild assumptions on (\mathcal{X}, μ) and (\mathcal{Y}, ν) and the cost function c (Villani et al., 2009). Moreover, this Kantorovich OT can be viewed as a relaxation of the Monge OT. When the optimal transport map T^* exists, the optimal transport plan π^* is given by the corresponding deterministic coupling, i.e., $\pi^* = (Id \times T^*) \# \mu$.

Neural Optimal Transport Neural Optimal Transport (Neural OT) approaches aim to learn optimal transport maps

using neural networks. Among them, the Semi-dual Neural OT (SNOT) methods leverage the semi-dual formulation of the OT problem (Rout et al., 2022; Fan et al., 2022; Choi et al., 2023; Makkula et al., 2020). Specifically, the Kantorovich problem admits the following semi-dual formulation (Villani et al., 2009, Thm. 5.10), (Santambrogio, 2015, Prop. 1.11):

$$S(\mu, \nu) := \sup_{V \in S_c} \left[\int_{\mathcal{X}} V^c(x) \mu(dx) + \int_{\mathcal{Y}} V(y) \nu(dy) \right], \quad (7)$$

where S_c denotes the set of c -concave functions $V : \mathcal{Y} \rightarrow \mathbb{R}$ and V^c denotes the c -transform of V , *i.e.*,

$$V^c(x) = \inf_{y \in \mathcal{Y}} [c(x, y) - V(y)]. \quad (8)$$

In SNOT, the transport map T_θ is parameterized to approximate the minimizer in the c -transform. By leveraging a correspondence between the c -transform V_ϕ^c and the transport network T_θ , we define:

$$T_\theta(x) \in \arg \min_{y \in \mathcal{Y}} [c(x, y) - V_\phi(y)] \quad (9)$$

$$\Leftrightarrow V_\phi^c(x) = c(x, T_\theta(x)) - V_\phi(T_\theta(x)). \quad (10)$$

This parameterization transforms the semi-dual formulation into a max-min optimization objective $\mathcal{L}(V_\phi, T_\theta)$:

$$\begin{aligned} & \sup_{V_\phi \in S_c} \inf_{T_\theta : \mathcal{X} \rightarrow \mathcal{Y}} \mathcal{L}(V_\phi, T_\theta) \quad \text{where} \quad \mathcal{L}(V, T) := \\ & \int_{\mathcal{X}} c(x, T(x)) - V(T(x)) \mu(dx) + \int_{\mathcal{Y}} V(y) \nu(dy). \end{aligned} \quad (11)$$

While existing SNOT approaches have primarily focused on finite-dimensional settings, this work generalizes this to infinite-dimensional Hilbert spaces, providing a rigorous treatment of neural transport in functional domains.

Spurious Solutions in SNOT Despite the success of SNOT models, the max-min objective has the **spurious solution problem** (Rout et al., 2022; Fan et al., 2023; Choi et al., 2025). This means that the max-min solution (V^*, T_{rec}) (Eq. 2 and 3) of the max-min objective function (Eq. 11) may not accurately recover the optimal transport map T^* . It is well-known that the true pair of Kantrovich potential and optimal transport map (V^*, T^*) is an optimal max-min solution, but not every solution recovers the true optimal transport map (Rout et al., 2022; Fan et al., 2023). In other words, T_{rec} may differ significantly from T^* while still satisfying the optimality conditions of the objective. A known sufficient condition for preventing spurious solutions in finite-dimensional settings is that the source measure μ must not assign positive mass to measurable sets with a Hausdorff dimension of at most $d - 1$ (Choi et al., 2025). This condition is satisfied, for instance, if μ is absolutely continuous with respect to the

Lebesgue measure. Our work generalizes this sufficient condition to **infinite-dimensional Hilbert spaces**, where the concept of Lebesgue measure is absent, and the geometry of singular measures is more complex.

3. Analytical Results for Semi-dual Neural OT in Hilbert spaces

We extend the Semi-dual Neural OT framework to infinite-dimensional Hilbert spaces and investigate the corresponding spurious solution problem. We first establish the foundational OT theory in Hilbert spaces (Section 3.1) and subsequently bridge these theoretical results with SNOT models (Section 3.2). Further analysis regarding ill-posedness, spurious solutions, and saddle points analysis of SNOT, accompanied by examples, can be found in Appendix G.

3.1. General OT on Hilbert Spaces

If \mathcal{X} and \mathcal{Y} are (potentially infinite-dimensional) Polish spaces and the cost function c is lower semi-continuous, an optimal transport plan π^* exists (*e.g.* (Santambrogio, 2015, Theorem 1.7)). On the other hand, additional structural assumptions on the source measure, such as a regular measure, are required to ensure that the optimal transport is realized by a deterministic map.

Regular Measure on Hilbert Spaces To address this issue on transport maps, the notion of a *regular measure* has been introduced (see, *e.g.*, (Ambrosio et al., 2005)). We begin by establishing the functional analytic framework, with a specific focus on Hilbert spaces and Gaussian measures.

Definition 3.1. Let H be a separable Hilbert space (possibly infinite-dimensional), and let $\mathcal{P}(H)$ denote the set of all probability measures on H . A measure $\mu \in \mathcal{P}(H)$ is **regular** if $\mu(N) = 0$ for every Gaussian null set N . We denote by $\mathcal{P}^r(H)$ the set of regular measures on H .

Refer to Appendix B for the formal definition of Gaussian null sets. In the finite-dimensional Euclidean case ($H = \mathbb{R}^d$), Gaussian null sets coincide with Lebesgue-negligible sets (see, *e.g.*, (Ambrosio et al., 2005)). Thus, a measure $\mu \in \mathcal{P}(\mathbb{R}^d)$ is regular (in the sense of Definition 3.1) if and only if it is absolutely continuous with respect to the Lebesgue measure ($\mu \ll \mathcal{L}^d$). In this sense, the **regular measure provides a rigorous generalization of absolute continuity for infinite-dimensional spaces** where the Lebesgue measure is unavailable.

OT on Hilbert Spaces In this work, we consider the OT problem with the **quadratic cost function**:

$$c(x, y) := \frac{1}{2} \|x - y\|_H^2. \quad (12)$$

To ensure the finiteness of the optimal transport cost, we restrict our analysis to probability measures with finite second moments. We denote the **Wasserstein space of order 2** as:

$$\mathcal{P}_2(H) := \left\{ \mu \in \mathcal{P}(H) : \int_H \|x\|_H^2 \mu(dx) < \infty \right\}. \quad (13)$$

Furthermore, we define the subclass of regular measures with finite second moments as $\mathcal{P}_2^r(H) := \mathcal{P}^r(H) \cap \mathcal{P}_2(H)$.

The notion of regular measure is essential in the infinite-dimensional setting. Specifically, the assumption $\mu \in \mathcal{P}_2^r(H)$ serves as a sufficient condition for the well-posedness of the Monge problem. This guarantees that the optimal transport can be realized by a unique deterministic map (Proposition C.1).

3.2. Connections to SNOT on Hilbert Spaces

Our goal is to extend the SNOT framework to Hilbert spaces. To this end, we follow the derivation of SNOT for finite-dimensional settings in Section 2. While the semi-dual formulation of OT (Eq. 7) remains valid for Hilbert spaces (Villani et al., 2009; Santambrogio, 2015; Ambrosio et al., 2005), the formal justification for the T_θ -parameterization in (Eq. 9) remains a critical theoretical gap. Specifically, we must establish that the **following optimality condition also holds in the Hilbert space setting**:

$$\{T^*(x)\} \subseteq \arg \min_{y \in H} [c(x, y) - V^*(y)]. \quad (14)$$

Note that although Proposition C.1 guarantees the existence of optimal solutions (V^*, T^*) , the direct link between these solutions and the max-min optimization objective (Eq. 1) remains under-explored in the infinite-dimensional setting.

Furthermore, the **well-posedness of this T_θ -parameterization, which prevents the spurious solutions**, is non-trivial. Establishing that the minimizer is unique—thereby ensuring T_{rec} is a single-valued function—requires a rigorous analysis leveraging the regular conditions of measures in Hilbert spaces.

To address this, we provide a **rigorous characterization of the Monge map** (Theorem 3.2) using functional variations.

Using the notion of Gâteaux differential (Eq. B.2), we prove that the minimizer of Eq. 15 is uniquely determined. This ensures that the T_θ parameterization is well-posed, *i.e.*, there are no spurious solutions. The proof is provided in Appendix C.2.

Theorem 3.2 (Characterization of Monge Map and Consistency of HiSNOT). *Consider the quadratic cost $c(x, y) = \frac{1}{2} \|x - y\|_H^2$ along with measures $\mu \in \mathcal{P}_2^r(H)$ and $\nu \in \mathcal{P}_2(H)$. Let V^* be a Kantorovich potential. Then, the following hold:*

(i) *The set of minimizers*

$$\mathcal{D}_x := \arg \min_{y \in \text{supp}(\nu)} [c(x, y) - V^*(y)] \quad (15)$$

is a singleton for μ -almost every $x \in H$. Specifically, there exists a unique element $y_x \in \mathcal{D}_x$ such that defining $T^(x) := y_x$ recovers the unique Monge map μ -almost surely.*

(ii) *Let (V^*, T^*) be an optimal max-min solution to the SNOT objective (Eq. 1). Then, T^* is the unique minimizer of the inner minimization problem:*

$$T^* = \arg \min_{T: H \rightarrow H} \mathcal{L}(V^*, T). \quad (16)$$

Then, T^ coincides with the unique Monge map μ -almost everywhere.*

4. Method

In this section, we propose a principled practical scheme to transform a singular source measure μ into a regular measure μ_Q , thereby ensuring the well-posedness of the SNOT framework in Hilbert spaces (Section 4.1). We then revisit the previously discussed spurious solution cases to demonstrate the efficacy of our approach (Section G.3). Finally, we introduce our SNOT framework for Hilbert space, called **Hilbert Semi-dual Neural Optimal Transport (HiSNOT)** (Section 4.2).

4.1. Gaussian Smoothing in Hilbert Spaces

To resolve the ill-posedness and overcome spurious solutions inherent in singular settings (Section G.1), we introduce a regularization strategy based on **Gaussian smoothing**. The core idea is to convolve the singular source measure with an appropriate Gaussian measure to satisfy the regular condition $\mathcal{P}^r(H)$.

To do so, we first formally define the Gaussian measures in the Hilbert space setting.

Definition 4.1 (Gaussian Measures). Gaussian measures on a separable Hilbert space H are characterized by their covariance operators:

- (i) An operator $Q : H \rightarrow H$ is called a **covariance operator** if it is bounded, linear, self-adjoint, positive (*i.e.*, $\langle Qx, x \rangle_H \geq 0$ for all $x \in H$), and trace-class (*i.e.*, $\sum_{k=1}^{\infty} \langle Qe_k, e_k \rangle_H < \infty$).
- (ii) A random variable $\mathbf{X} : \Omega \rightarrow H$ is an **H -valued Gaussian random vector** if $\langle X, x \rangle_H$ is a real Gaussian random variable for every $x \in H$. In this case, there exist a mean vector $m \in H$ and a covariance operator Q such that $\mathbf{X} \sim \mathcal{N}(m, Q)$, meaning

$$\langle \mathbf{X}, x \rangle_H \sim \mathcal{N}(\langle m, x \rangle_H, \langle Qx, x \rangle_H), \quad \forall x \in H.$$

Formally, let μ be the source measure. We define the **Gaussian smoothed measure** $\mu_Q = \mu * \gamma$ as the convolution of μ and a Gaussian measure $\gamma = \mathcal{N}(0, Q)$:

$$(\mu * \gamma)(A) := \int_H \mu(A - x)\gamma(dx).$$

Practically, this corresponds to perturbing the random variable $\mathbf{X} \sim \mu$ with independent Gaussian noise:

$$\mathbf{X}^\gamma := \mathbf{X} + \xi, \quad \text{where } \xi \sim \mathcal{N}(0, Q).$$

Here, the **covariance operator Q plays a decisive role**, as it determines the **directions and magnitude of the smoothing**. Through its spectral decomposition $Qe_k = \lambda_k e_k$, the operator Q specifies that the noise is injected along the eigen-directions $\{e_k\}$ with variances $\{\lambda_k\}$. Therefore, choosing Q is equivalent to selecting the geometry of the regularization: if $\lambda_k > 0$, the smoothing is active in the direction e_k ; if $\lambda_k = 0$ (i.e., $e_k \in \text{Ker}(Q)$), no smoothing occurs in that direction.

Convergence of Smoothed Monge Maps The strategy of using regularized measures is theoretically justified by the following convergence result, whose proof is provided in Appendix E:

Theorem 4.2. *Let $\{\mu_k\}_{k \in \mathbb{N}}$ be a sequence of probability measures in $\mathcal{P}_2^r(H)$, and let T_k^* denote the unique optimal transport map from μ_k to ν . If μ_k converges to μ in the Wasserstein metric W_2 as $k \rightarrow \infty$, then there exist a subsequence $\{k_n\}_{n \in \mathbb{N}}$ and an optimal transport plan $\pi \in \Pi(\mu, \nu)$ such that the associated plans $\pi_{k_n}^* = (Id \times T_{k_n}^*)_\# \mu_{k_n}$ converge weakly to π^* .*

Importantly, the limit measure μ is not required to be regular. In cases where μ is singular, the existence of a Monge map is not guaranteed; only an optimal transport plan π^* exists. Theorem 4.2 addresses this by guaranteeing that π^* can be recovered as the limit of unique Monge maps T_k^* derived from regularized approximations (e.g., via Gaussian smoothing). This theoretical result directly validates our annealing strategy proposed in Section 4.2, representing a Hilbert space generalization of the finite-dimensional framework established by Choi et al. (2025).

Characterization of Necessary Smoothing We further establish a **necessary and sufficient** condition for the smoothed measure $\mu * \gamma$ to satisfy the regular condition. This result characterizes how the covariance Q (specifically, its kernel) determines the success of the smoothing. Note that this characterization was not established in (Choi et al., 2025), and it provides the finite-dimensional Euclidean case as a direct corollary.

Theorem 4.3. *Let γ be a centered Gaussian measure with a covariance operator Q , and let $\mu \in \mathcal{P}(H)$. Then, the convolution $\gamma * \mu$ belongs to $\mathcal{P}^r(H)$ if and only if the projection*

of μ onto the kernel of Q is regular, i.e., $\mu_K \in \mathcal{P}^r(\text{Ker}(Q))$. Here, the projected measure $\mu_K(B)$ is defined as:

$$\mu_K(B) := \mu(\{h \in H : \pi_K(h) \in B\}).$$

where $\pi_K : H \rightarrow \text{Ker}(Q)$ denotes the orthogonal projection.

Theorem 4.3 proves that the smoothed measure becomes regular if and only if the injected noise covers all singular directions of μ . This ensures the existence of a unique Monge map for the regularized problem. Combined with Theorem 4.2, this provides a principled mechanism to recover the true optimal transport plan in the limit as the noise amplitude vanishes.

4.2. Our HiSNOT Framework

Our **Hilbert Semi-dual Neural Optimal Transport (HiSNOT)** framework is the first attempt to generalize the Semi-dual Neural Optimal Transport (SNOT) framework to infinite-dimensional Hilbert spaces. (Section 4.2.1) Moreover, we propose an annealed Gaussian smoothing scheme to ensure the well-posedness of the SNOT objective and the recovery of the optimal transport plan (Section 4.2.2).

4.2.1. GENERALIZATION OF SNOT TO HILBERT SPACES

While SNOT has traditionally been applied to finite-dimensional Euclidean spaces (Rout et al., 2022; Fan et al., 2023; Makkula et al., 2020), we generalize the framework to operate on a separable Hilbert space H . We parameterize the transport map $T_\theta : H \rightarrow H$ and the potential $V_\phi : H \rightarrow \mathbb{R}$ as functional operators acting on H (Eq. 9), which leads to the following functional max-min objective:

$$\sup_{V_\phi \in S_c} \inf_{T_\theta : H \rightarrow H} \mathcal{L}(V_\phi, T_\theta) \quad \text{where} \quad \mathcal{L}(V, T) := \int_{\mathcal{X}} c(x, T(x)) - V(T(x)) \mu(dx) + \int_{\mathcal{Y}} V(y) \nu(dy). \quad (17)$$

where $c(x, y) = \frac{1}{2} \|x - y\|_H^2$. Note that this objective has exactly the same form except that $T_\theta : H \rightarrow H$. Our contribution lies in theoretically proving that this T_θ -parameterization remains valid in Hilbert spaces (Theorem 3.2). Unlike Euclidean SNOT, the transport map T_θ must now be capable of mapping functions to functions (e.g., through Neural Operators (Kovachki et al., 2023)). In our implementation, we adopt the Fourier Neural Operator architectures (Li et al., 2020).

4.2.2. LEARNING OPTIMAL TRANSPORT PLAN VIA ANNEALED GAUSSIAN SMOOTHING

To learn the true optimal transport plan π^* between a potentially singular source μ and a target ν , we propose an

Annealed Gaussian Smoothing strategy based on the HiSNOT framework. This method utilizes our theoretical results in Section 3.1 to ensure that the neural networks optimize a well-posed objective without spurious solutions at every stage of training.

Intuitively, our method is to **construct a sequence of regularized source measures $\{\mu_{\epsilon_n}\}$ where the noise level ϵ_n is gradually annealed to zero**. For any $\epsilon > 0$, we define the smoothed measure as the convolution $\mu_\epsilon := \mu * \mathcal{N}(0, \epsilon^2 Q)$. As established in Theorem 3.2, this convolution transforms a singular measure into a regular measure ($\mu_\epsilon \in \mathcal{P}_2^r(H)$), provided the covariance operator Q covers the singular directions of μ . This makes the HiSNOT objective at each noise level well-posed, thereby increasing the training stability and providing guarantees to recovering the true Monge map. By Theorem 4.2, as $\epsilon \rightarrow 0$, the sequence of maps $\{T_{\epsilon_n}^*\}$ is guaranteed to converge toward the original optimal transport plan π^* . See Algorithm 1 for details.

$$\sup_{V_\phi \in S_c} \inf_{T_\theta: H \rightarrow H} \mathcal{L}_n(V_\phi, T_\theta) \quad \text{where} \quad \mathcal{L}_n(V, T) := \int_{\mathcal{X}} c(x, T(x)) - V(T(x)) \mu_{\epsilon_n}(dx) + \int_{\mathcal{Y}} V(y) \nu(dy). \quad (18)$$

Practical Smoothing via Spectral Augmentation Here, we provide a detailed explanation of how to actually implement Gaussian smoothing in practice via examples. In Hilbert spaces such as $H = L^2(0, 1)$, we implement the **Gaussian smoothing $\mathcal{N}(0, \epsilon^2 Q)$ by injecting noise into the spectral coefficients** of the source data. This ensures that the regularization is geometrically aligned with the functional structure of the data.

Let $\{e_k\}_{k \in \mathbb{N}}$ be an orthonormal basis of H (e.g., Fourier or Haar wavelet basis) and let $\{\lambda_k\}_{k \in \mathbb{N}}$ be a summable sequence of non-negative components, i.e., $\sum_k \lambda_k < \infty$ (For instance, $\lambda_k = 1/k^2$). We construct H -valued Gaussian noise via the following proposition. The proof can be found in Appendix F.

Proposition 4.4. *Let $\{e_k\}_{k \in \mathbb{N}}$ be an orthonormal basis of H . For a summable sequence $\{\lambda_k\}_{k \in \mathbb{N}} \subset [0, \infty)$ and i.i.d. standard Gaussian variables $\{\xi_k\}$*

$$X := \sum_{k=1}^{\infty} \sqrt{\lambda_k} \xi_k e_k \quad \text{where } \xi_k \sim \text{i.i.d. } \mathcal{N}(0, 1) \quad (19)$$

is a H -valued Gaussian random vector with zero mean, and a trace-class operator Q defined in (Eq. 30).

During training, for each source sample $\mathbf{x} \sim \mu$, we generate a smoothed sample $\mathbf{x}_\epsilon \sim \mu_\epsilon$ through the following process:

1. Project \mathbf{x} onto the chosen basis to obtain coefficients $c_k = \langle \mathbf{x}, e_k \rangle_H$.

2. Add weighted Gaussian noise to each coefficient: $\hat{c}_k = c_k + \epsilon \sqrt{\lambda_k} \zeta_k$.
3. Form the smoothed sample $\mathbf{x}_\epsilon = \sum_k \hat{c}_k e_k$.

The basis examples $\{e_k\}_{k \in \mathbb{N}}$ are included in Appendix F.

Annealing Schedule We initialize the training with a sufficiently large ϵ_{\max} . As the training progresses, we decay ϵ according to an annealing schedule. Specifically, following (Choi et al., 2025), we employ a linear interpolation annealing from σ_{\max} to σ_{\min} . This allows the transport map T_θ to first capture the coarse global structure of the transport plan and then refine the mapping as the source measure converges back to its original singular support.

5. Experiments

We empirically validate our theoretical analysis on Semi-dual Neural OT on Hilbert spaces through the following experiments:

- In Sec 5.1, we evaluate the effectiveness of Gaussian smoothing in overcoming spurious solutions.
- In Sec 5.2, we empirically test our characterization theorem for smoothing operators (Theorem 4.3) by comparing theoretically appropriate operators and inappropriate operators.
- In Sec 5.3, we assess our SNOT model on time-series imputation benchmarks, which are real-world applications for high-dimensional function space datasets.

For implementation details of experiments, please refer to Appendix H.

5.1. Effect of Gaussian Smoothing on Spurious Solutions

We empirically verify the effectiveness of Gaussian smoothing, proved in 3.2, by evaluating under the spurious solution examples described in Section G.1. Specifically, we compare the vanilla HiSNOT model (Eq. 17) and the regularized version utilizing Gaussian smoothing (Eq. 18). In these settings, the vanilla model is exposed to ill-posedness and spurious solution problems. In contrast, the regularized model introduces principled Gaussian smoothing with a noise level ϵ . This leads to the well-posed learning objective that eliminates spurious solutions. The evaluation is conducted on synthetic datasets, including Perpendicular (Example 1) and One-to-Many (Example 2) (See Appendix G.2 for details). Here, we utilize two metrics: the transport cost error $D_{cost} = |W_2^2(\mu, \nu) - \int \|T_\theta(x) - x\|^2 d\mu(x)|$ and the target distribution error $D_{target} = W_2^2(T_\theta \# \mu, \nu)$. D_{cost} measures how closely the model approximates the theoretically optimal transport cost, while D_{target} measures how accurately the model generates the target distribution.

The results are provided in Figure 1 and Table 1. While the

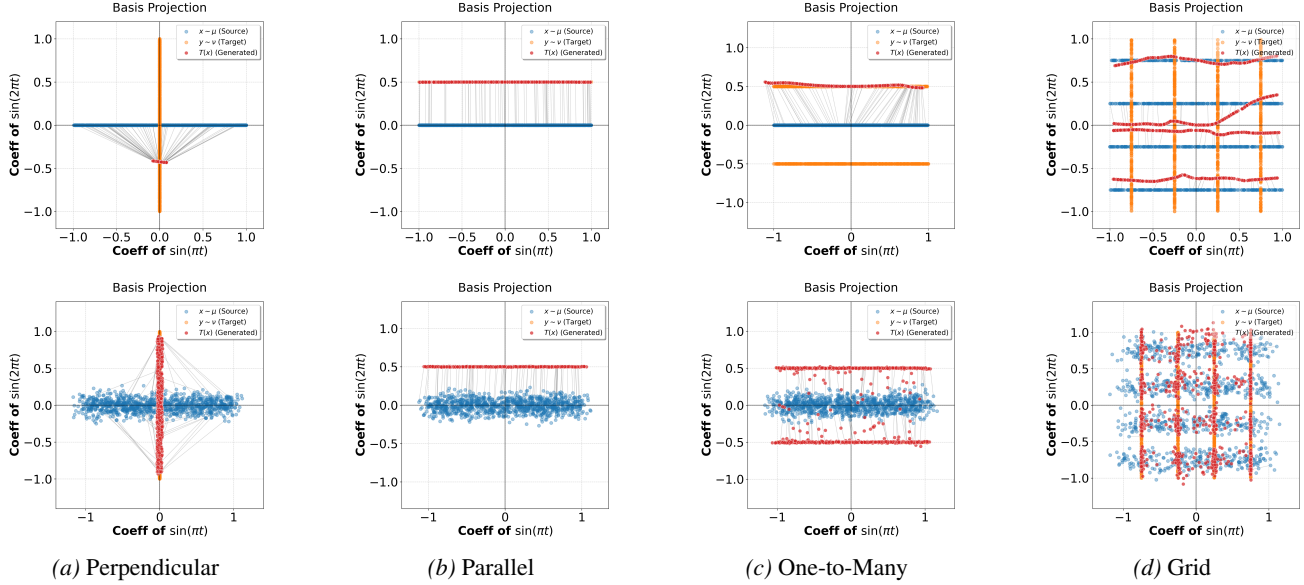


Figure 1. Comparison of transport maps learned by vanilla HiSNOT (top row) and HiSNOT with annealed smoothing (bottom row). The vanilla model exhibits spurious solutions in singular cases (Perpendicular, One-to-Many, Grid), while our proposed smoothing correctly recovers the optimal transport plan.

Table 1. Quantitative comparison of HiSNOT performance with and without Gaussian smoothing across synthetic scenarios. We report the transport cost error $D_{\text{cost}}(\downarrow)$ and target distribution error $D_{\text{target}}(\downarrow)$. The inclusion of smoothing (3) effectively resolves singular measures, significantly reducing errors due to spurious solutions.

| Smoothing | Perpendicular | | Parallel | | One-to-Many | | Grid | |
|-----------|-------------------|---------------------|-------------------|---------------------|-------------------|---------------------|-------------------|---------------------|
| | D_{cost} | D_{target} | D_{cost} | D_{target} | D_{cost} | D_{target} | D_{cost} | D_{target} |
| ✗ | 0.101 | 0.249 | 0.001 | 0.000 | 0.051 | 0.288 | 0.007 | 0.031 |
| ✓ | 0.038 | 0.006 | 0.003 | 0.001 | 0.001 | 0.004 | 0.007 | 0.008 |

baseline HiSNOT exhibits spurious solutions and fails to accurately reconstruct the target measure, our regularized model faithfully learns the optimal transport plan. Quantitatively, our model is significantly more accurate in the Perpendicular, One-to-Many, and Grid tasks. Specifically, in the Perpendicular data, the introduction of Gaussian smoothing significantly reduces the transport cost error D_{cost} from 0.101 to 0.038 and the target distribution error D_{target} from 0.249 to 0.006. Interestingly, in the Parallel data, the unregularized model performs well. Thus, both models achieve results with competitive accuracy.

5.2. Characterization of Smoothing Operator

Theorem 4.3 establishes the necessary and sufficient conditions for a Gaussian covariance operator to transform a singular source measure μ into a regular measure via convolution smoothing (*i.e.*, $\gamma * \mu$). This condition requires the Gaussian measure γ to have non-zero variance along every eigen-direction where the source measure μ is singular.

To empirically validate this, we compare (1) theoretically appropriate Gaussian smoothing against (2) inappropriate Gaussian smoothing using the Perpendicular dataset. In this

setting, the source measure μ is regular specifically along the eigen-direction $\{\sin(\pi t)\}$ but remains singular along all other directions. We evaluate two Gaussian measures:

- **Appropriate smoothing** (γ_1) such that $\text{Ker}(Q_1) = \text{span}\{\sin(\pi t)\}$. This operator avoids smoothing only in the direction where μ is already regular, thereby satisfying the theorem.
- **Inappropriate smoothing** (γ_2) such that $\text{Ker}(Q_2) = \text{span}\{\sin(2\pi t)\}$. This operator fails to apply smoothing to a direction where μ is singular, thus failing to produce a regular measure.

Figure 2 presents the qualitative comparison of these two smoothings. With appropriate smoothing (left), the HiSNOT model successfully captures the target data distribution, as observed in the full-space regularization experiments (Figure 1). However, under the appropriate smoothing (right), the HiSNOT exhibits the spurious solution patterns. These results empirically verify our characterization of the necessary smoothing result (Theorem 4.3). For regularization, the noise distribution must explicitly cover the singularities of the source measure to ensure a well-posedness.

Table 2. Unpaired time-series imputation performance (MSE and MAE) across five datasets. Results are averaged over missing ratios of 0.5 and 0.7. The **bold** and underlined values denote the best and second-best results. All baseline results are taken from Wang et al. (2025).

| Datasets | ETTh1 | | ETTh2 | | ETTm1 | | ETTm2 | | Exchange | | |
|------------------------------------|---------|--------------|--------------|--------------|--------------|--------------|--------------|--------------|--------------|--------------|--------------|
| | Methods | MSE | MAE |
| Transformer (Vaswani et al., 2017) | | 0.338 | 0.410 | 0.282 | 0.383 | 0.085 | 0.196 | 0.056 | 0.161 | 0.320 | 0.289 |
| DLinear (Zeng et al., 2023) | | <u>0.187</u> | 0.307 | 0.138 | 0.262 | 0.131 | 0.250 | 0.107 | 0.227 | 0.288 | 0.238 |
| TimesNet (Wu et al., 2022) | | 0.343 | 0.415 | 0.147 | 0.278 | 0.086 | 0.209 | 0.093 | 0.220 | 0.372 | 0.308 |
| FreTS (Yi et al., 2023) | | 0.233 | 0.355 | 0.159 | 0.278 | 0.061 | 0.168 | 0.040 | 0.136 | 0.229 | 0.189 |
| PatchTST (Nie, 2022) | | 0.216 | 0.338 | 0.144 | 0.272 | 0.055 | 0.153 | 0.033 | 0.122 | 0.227 | 0.188 |
| SCINet (Liu et al., 2022) | | 0.195 | 0.321 | 0.172 | 0.288 | 0.088 | 0.204 | 0.085 | 0.211 | 0.326 | 0.269 |
| iTransformer (Liu et al., 2023) | | 0.206 | 0.321 | 0.125 | 0.237 | 0.068 | 0.173 | 0.043 | 0.142 | 0.087 | 0.070 |
| SAITS (Du, 2023) | | 0.286 | 0.358 | 0.236 | 0.303 | 0.079 | 0.188 | 0.059 | 0.160 | 1.007 | 0.832 |
| CSDI (Tashiro et al., 2021) | | <u>0.187</u> | 0.303 | 0.107 | 0.271 | 0.156 | 0.206 | 0.161 | 0.150 | 0.134 | 0.150 |
| Sinkhorn (Muzellec et al., 2020) | | 0.936 | 0.685 | 0.877 | 0.644 | 0.965 | 0.717 | 0.927 | 0.702 | 0.783 | 0.648 |
| TDM (Zhao et al., 2023) | | 0.991 | 0.749 | 0.998 | 0.745 | 1.003 | 0.756 | 0.998 | 0.748 | 0.969 | 0.801 |
| PWS-I (Wang et al., 2025) | | 0.160 | 0.262 | <u>0.053</u> | 0.155 | <u>0.057</u> | 0.146 | <u>0.025</u> | 0.103 | 0.036 | 0.030 |
| HiSNOT (Ours) | | 0.215 | <u>0.288</u> | 0.048 | 0.144 | 0.066 | 0.150 | 0.021 | 0.089 | 0.004 | 0.042 |

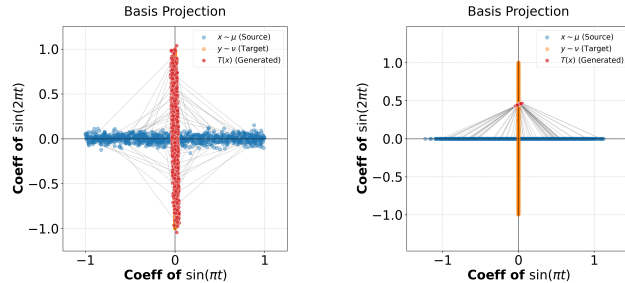


Figure 2. Empirical validation of Theorem 4.3. **Left:** Appropriate smoothing covers singular directions, leading to a unique Monge map. **Right:** Inappropriate smoothing fails to cover singular directions, resulting in spurious solutions.

5.3. Time Series Imputation Benchmarks

We evaluate HiSNOT with Smoothing on unpaired time series imputation benchmarks. Time-series data is one of the most widely used benchmarks for machine learning models operating on functional data (Ramsay & Silverman, 2005; Jiang et al., 2025). For time-series data, (possibly irregular) observations are regarded as discrete samples from underlying continuous processes defined in a Hilbert space. Here, we treat the imputation task as an optimal transport problem between the distribution of partially observed sequences (source) and fully observed paths (target).

Real-world time series data often reside on low-dimensional manifolds (*Manifold Hypothesis*), which implies that partially observed data also follows a singular measure. This makes standard SNOT prone to spurious solutions. By applying HiSNOT with annealed smoothing, we address these singular distributions. This experiment assesses the practical utility of HiSNOT in high-dimensional, real-world scenarios where the data inherently possesses functional structures. The imputation performance is evaluated through the Mean Absolute Error (MAE) and Mean Squared Error (MSE) following (Wang et al., 2025).

The results in Table 2 demonstrate that HiSNOT consis-

tently achieves state-of-the-art or competitive performance across all benchmarks. Our model achieves the best performance in MSE and MAE for ETTh2, ETTm2, and Exchange datasets, and the second-best performance in several other categories. Specifically, on the Exchange dataset, our model significantly outperforms all baselines in MSE, achieving a value of 0.004, which is an order of magnitude lower than the second-best performer, PWS-I (0.036). Compared to classical OT baselines such as Sinkhorn and TDM, HiSNOT provides a significant improvement in accuracy, achieving better or comparable to previous state-of-the-art method (Wang et al., 2025).

6. Conclusion

We introduce **HiSNOT**, the first generalization of the Semi-dual Neural Optimal Transport (SNOT) framework to infinite-dimensional Hilbert spaces. We provide the first theoretical analysis of spurious solutions in Hilbert spaces. Based on these, we propose a principled method for learning the true optimal transport plan when a Monge map does not exist. Our contributions include a rigorous treatment of Gaussian smoothing techniques for transforming singular measures into regular ones, and the derivation of a necessary and sufficient condition for the Gaussian covariance operators required for well-posedness. Our experiments demonstrate that our proposed annealed smoothing method successfully addresses failure cases and achieves state-of-the-art results in real-world functional applications. One limitation of our work is that our convergence guarantee (Theorem 4.2) holds up to a subsequence. This is an inherent characteristic of the ill-posed nature of OT problems where the optimal plan π^* may not be unique; thus, the sequence may oscillate between valid solutions. Nevertheless, our theorem ensures that any limit point obtained from training is a valid optimal transport plan. Empirically, our gradual training scheme exhibited stable convergence behavior in all experiments.

Acknowledgements

J.-H. Choi was supported by a KIAS Individual Grant (MG102701) at the Korea Institute for Advanced Study. J. Yoon and J. W. Choi were partially supported by the National Research Foundation of Korea (NRF) grant funded by the Korea government (MSIT) (No. RS-2024-00349646). D. Kwon is partially supported by the National Research Foundation of Korea (NRF) grant funded by the Korea government (MSIT) (No. RS-2023-00252516 and No. RS-2024-00408003), the POSCO Science Fellowship of POSCO TJ Park Foundation, and the Korea Institute for Advanced Study. J. W. Choi and D. Kwon thank the Center for Advanced Computation in KIAS for providing computing resources.

Impact Statement

This paper presents work whose goal is to advance the field of Machine Learning. There are many potential societal consequences of our work, none which we feel must be specifically highlighted here.

References

Ambrosio, L., Gigli, N., and Savaré, G. *Gradient flows: in metric spaces and in the space of probability measures*. Springer, 2005.

Brenier, Y. Polar factorization and monotone rearrangement of vector-valued functions. *Communications on pure and applied mathematics*, 44(4):375–417, 1991.

Choi, J., Choi, J., and Kang, M. Generative modeling through the semi-dual formulation of unbalanced optimal transport. In *Thirty-seventh Conference on Neural Information Processing Systems*, 2023.

Choi, J., Choi, J., and Kwon, D. Overcoming spurious solutions in semi-dual neural optimal transport: A smoothing approach for learning the optimal transport plan. In *Forty-second International Conference on Machine Learning*, 2025.

Chu, R., Choi, J., and Kwon, D. Rate-optimal noise annealing in semi-dual neural optimal transport: Tangential identifiability, off-manifold ambiguity, and guaranteed recovery. *arXiv preprint arXiv:2602.04110*, 2026.

Conway, J. B. *A course in functional analysis*. Springer, 2019.

Du, W. Pypots: a python toolbox for data mining on partially-observed time series. *arXiv preprint arXiv:2305.18811*, 2023.

Fan, J., Liu, S., Ma, S., Chen, Y., and Zhou, H.-M. Scalable computation of monge maps with general costs. In *ICLR Workshop on Deep Generative Models for Highly Structured Data*, 2022.

Fan, J., Liu, S., Ma, S., Zhou, H.-M., and Chen, Y. Neural monge map estimation and its applications. *Transactions on Machine Learning Research*, 2023. ISSN 2835-8856. URL <https://openreview.net/forum?id=2mZSlQscj3>. Featured Certification.

Gangbo, W. and McCann, R. J. The geometry of optimal transportation. *Acta Mathematica*, 177(2):113–161, 1996.

Hairer, M. An introduction to stochastic pdes. *arXiv preprint arXiv:0907.4178*, 2009.

Jiang, S., Hu, Y., Li, W., and Zeng, P. Deepfrc: An end-to-end deep learning model for functional registration and classification. *arXiv preprint arXiv:2501.18116*, 2025.

Kantorovich, L. V. On a problem of monge. *Uspekhi Mat. Nauk*, pp. 225–226, 1948.

Kim, M., Hioka, Y., and Witbrock, M. Neural fourier modelling: A highly compact approach to time-series analysis. *arXiv preprint arXiv:2410.04703*, 2024.

Kovachki, N., Li, Z., Liu, B., Azizzadenesheli, K., Bhattacharya, K., Stuart, A., and Anandkumar, A. Neural operator: Learning maps between function spaces with applications to pdes. *Journal of Machine Learning Research*, 24(89):1–97, 2023.

Li, Z., Kovachki, N., Azizzadenesheli, K., Liu, B., Bhattacharya, K., Stuart, A., and Anandkumar, A. Fourier neural operator for parametric partial differential equations. *arXiv preprint arXiv:2010.08895*, 2020.

Liu, M., Zeng, A., Chen, M., Xu, Z., Lai, Q., Ma, L., and Xu, Q. Scinet: Time series modeling and forecasting with sample convolution and interaction. *Advances in Neural Information Processing Systems*, 35:5816–5828, 2022.

Liu, Y., Hu, T., Zhang, H., Wu, H., Wang, S., Ma, L., and Long, M. itransformer: Inverted transformers are effective for time series forecasting. *arXiv preprint arXiv:2310.06625*, 2023.

Makkuva, A., Taghvaei, A., Oh, S., and Lee, J. Optimal transport mapping via input convex neural networks. In *International Conference on Machine Learning*, pp. 6672–6681. PMLR, 2020.

Monge, G. Mémoire sur la théorie des déblais et des remblais. *Mem. Math. Phys. Acad. Royale Sci.*, pp. 666–704, 1781.

Muzellec, B., Josse, J., Boyer, C., and Cuturi, M. Missing data imputation using optimal transport. In *International Conference on Machine Learning*, pp. 7130–7140. PMLR, 2020.

Nie, Y. A time series is worth 64words: Long-term forecasting with transformers. *arXiv preprint arXiv:2211.14730*, 2022.

Rahman, M. A., Florez, M. A., Anandkumar, A., Ross, Z. E., and Azizzadenesheli, K. Generative adversarial neural operators. *arXiv preprint arXiv:2205.03017*, 2022.

Ramsay, J. O. and Silverman, B. W. *Functional data analysis*. Springer, 2005.

Rout, L., Korotin, A., and Burnaev, E. Generative modeling with optimal transport maps. In *International Conference on Learning Representations*, 2022.

Rudin, W. *Real and complex analysis*. McGraw-Hill, Inc., 1987.

Santambrogio, F. Optimal transport for applied mathematicians. *Birkhäuser, NY*, 55(58-63):94, 2015.

Tashiro, Y., Song, J., Song, Y., and Ermon, S. Csd: Conditional score-based diffusion models for probabilistic time series imputation. *Advances in neural information processing systems*, 34:24804–24816, 2021.

Vaswani, A., Shazeer, N., Parmar, N., Uszkoreit, J., Jones, L., Gomez, A. N., Kaiser, Ł., and Polosukhin, I. Attention is all you need. *Advances in neural information processing systems*, 30, 2017.

Villani, C. et al. *Optimal transport: old and new*, volume 338. Springer, 2009.

Wang, H., Li, H., Chen, X., Gong, M., Chen, Z., et al. Optimal transport for time series imputation. In *The Thirteenth International Conference on Learning Representations*, 2025.

Wang, J.-L., Chiou, J.-M., and Müller, H.-G. Functional data analysis. *Annual Review of Statistics and Its Application*, 3(Volume 3, 2016): 257–295, 2016. ISSN 2326-831X. doi: <https://doi.org/10.1146/annurev-statistics-041715-033624>. URL <https://www.annualreviews.org/content/journals/10.1146/annurev-statistics-041715-033624>.

Wu, H., Xu, J., Wang, J., and Long, M. Autoformer: Decomposition transformers with auto-correlation for long-term series forecasting. *Advances in neural information processing systems*, 34:22419–22430, 2021.

Wu, H., Hu, T., Liu, Y., Zhou, H., Wang, J., and Long, M. Timesnet: Temporal 2d-variation modeling for general time series analysis. *arXiv preprint arXiv:2210.02186*, 2022.

Yi, K., Zhang, Q., Fan, W., Wang, S., Wang, P., He, H., An, N., Lian, D., Cao, L., and Niu, Z. Frequency-domain mlps are more effective learners in time series forecasting. *Advances in Neural Information Processing Systems*, 36: 76656–76679, 2023.

Zeng, A., Chen, M., Zhang, L., and Xu, Q. Are transformers effective for time series forecasting? In *Proceedings of the AAAI conference on artificial intelligence*, volume 37, pp. 11121–11128, 2023.

Zhao, H., Sun, K., Dezfouli, A., and Bonilla, E. V. Transformed distribution matching for missing value imputation. In *International Conference on Machine Learning*, pp. 42159–42186. PMLR, 2023.

A. Algorithm

Algorithm 1 Training algorithm of HiSNOT with Gaussian Annealing

Require: Source measure μ , target measure ν ; Orthonormal basis $\{e_k\}$ and summable sequence $\{\lambda_k\}$; Transport operator T_θ and potential V_ϕ ; Iterations K , inner-loop steps K_T ; Annealing schedule $\{\epsilon_k\}_{k=0}^K$.

- 1: **for** $k = 0, 1, 2, \dots, K$ **do**
- 2: Sample batches $\{x_i\}_{i=1}^n \sim \mu$ and $\{y_i\}_{i=1}^n \sim \nu$.
- 3: Generate H -valued Gaussian noise: $\xi = \sum_{j=1}^{\infty} \sqrt{\lambda_j} \zeta_j e_j$ where $\zeta_j \sim \mathcal{N}(0, 1)$.
- 4: Apply Spectral Smoothing
- 5: $\tilde{x} \leftarrow x + \epsilon_k \xi$.
- 6: Update ϕ to maximize:
- 7: $\mathcal{L}_\phi = \frac{1}{n} \sum_{i=1}^n [-V_\phi(T_\theta(\tilde{x}_i)) + V_\phi(y_i)]$.
- 8: **for** $j = 0, 1, \dots, K_T$ **do**
- 9: Sample a batch $\{x_i\}_{i=1}^n \sim \mu$ and generate new noise ξ .
- 10: $\tilde{x} \leftarrow x + \epsilon_k \xi$.
- 11: Update θ to minimize:
- 12: $\mathcal{L}_\theta = \frac{1}{n} \sum_{i=1}^n [\frac{1}{2} \|\tilde{x}_i - T_\theta(\tilde{x}_i)\|_H^2 - V_\phi(T_\theta(\tilde{x}_i))]$.
- 13: **end for**
- 14: **end for**

B. Definitions

Definition B.1. Let H be a separable Hilbert space (possibly infinite-dimensional), and let $\mathcal{P}(H)$ denote the set of all probability measures on H .

(i) A measure $\mu \in \mathcal{P}(H)$ is a *nondegenerate Gaussian measure* if for any $h \in H \setminus \{0\}$, the projection $\langle h, x \rangle_H$ has strictly positive variance. Specifically, there exist $m_h \in \mathbb{R}$ and $\sigma_h > 0$ such that for any interval $(a, b) \subset \mathbb{R}$:

$$\mu(\{x \in H : a < \langle h, x \rangle_H < b\}) = \frac{1}{\sqrt{2\pi\sigma_h^2}} \int_a^b \exp\left(-\frac{(t - m_h)^2}{2\sigma_h^2}\right) dt. \quad (20)$$

(ii) A Borel set $N \in \mathcal{B}(H)$ is called a *Gaussian null set* if $\mu(N) = 0$ for every nondegenerate Gaussian measure μ on H .

(iii) A measure $\mu \in \mathcal{P}(H)$ is *regular* if $\mu(N) = 0$ for every Gaussian null set N . We denote by $\mathcal{P}^r(H)$ the set of regular measures on H .

Because standard calculus is insufficient for infinite-dimensional spaces, we employ the *Gâteaux differential*. This generalizes the directional derivative to Banach spaces, providing the necessary mathematical tools to rigorously capture functional variations.

Definition B.2 (Gâteaux Differential). Let H be a Hilbert space, and $J : H \rightarrow \mathbb{R}$ be a real-valued functional. The Gâteaux differential of J at $x \in H$ in the direction $y \in H$ is defined as the limit:

$$\nabla_x J(x; y) := \lim_{\epsilon \rightarrow 0} \frac{J(x + \epsilon y) - J(x)}{\epsilon}, \quad (21)$$

provided the limit exists. If the limit exists for all directions $y \in H$, then J is said to be Gâteaux differentiable at x . Moreover, if J is Gâteaux differentiable at x , then for convenience, we omit the direction y .

C. Proof of Theorem 3.2

Proposition C.1 (Monge and its dual problems in Hilbert space). *Let $\mu \in \mathcal{P}_2^r(H)$, $\nu \in \mathcal{P}_2(H)$, and $c(x, y) = \frac{1}{2} \|x - y\|_H^2$. There exists a unique Monge map $T^* : H \rightarrow H$ in (Eq. 5), i.e., $T^*_\# \mu = \nu$. Also, the dual problem (Eq. 7) admits an optimal potential $V^* \in S_c$.*

Proposition C.1 generalizes **Brenier's classical result on the characterization of optimal maps** to the Hilbert space setting and is derived directly from (Ambrosio et al., 2005, Theorem 6.2.10).

C.1. Proof of Proposition C.1

First, we prove the well-posedness of Monge map.

Step 1. Existence of a Monge map T^ .*

By (Ambrosio et al., 2005, Theorem 6.2.10), for the quadratic cost

$$c(x, y) = \frac{1}{2} \|x - y\|^2,$$

there exists a unique optimal transport plan $\pi^* \in \Pi(\mu, \nu)$, and it is induced by a measurable transport map $T^* \in L^2(H, \mu; H)$:

$$\pi^* = (Id \times T^*)_\# \mu.$$

Step 2. Uniqueness of a Monge map T^ .*

Assume $T_1^*, T_2^* \in L^2(H, \mu; H)$ are two Monge maps such that

$$(Id \times T_1^*)_\# \mu = \pi^* = (Id \times T_2^*)_\# \mu.$$

Define a probability measure

$$\tilde{\mu}_x := \frac{1}{2} (\delta_{T_1^*(x)} + \delta_{T_2^*(x)}) \quad \text{and} \quad \bar{\pi} := \tilde{\mu}_x \otimes \mu(dx).$$

Since T_1^* and T_2^* are optimal,

$$\int_{H \times H} c(x, y) \bar{\pi}(dx, dy) = \int_H \frac{c(x, T_1^*(x)) + c(x, T_2^*(x))}{2} \mu(dx) = \int_H c(x, T_1^*(x)) \mu(dx) = C(\mu, \nu),$$

where C is the primal cost. $\bar{\pi} \in \Pi(\mu, \nu)$, $\bar{\pi}$ is also an optimal transport plan which is not induced by any transport map. This is a contradiction to (Ambrosio et al., 2005, Theorem 6.2.10). Hence $T_1^* = T_2^*$ μ -almost surely.

Now, we prove the existence of optimal potential $V^* \in S_c$. By (Ambrosio et al., 2005, Theorem 6.1.5), there exists a maximizing pair $(V^*, (V^*)^c)$ such that

$$(V^*)^c(x) + V^*(y) = c(x, y) \quad \pi^*\text{-a.e. in } H \times H.$$

Therefore, there exists a null set $N \subset H \times H$ such that for all $(x, y) \in H \times H \setminus N$, $(V^*)^c(x) + V^*(y) = c(x, y)$. By Step 1 in the proof of Theorem C.1,

$$0 = \pi(N) = \mu((Id \times T^*)^{-1}(N)),$$

where

$$(Id \times T^*)^{-1}(N) = \{x \in H : (x, T^*(x)) \in N\} =: N_1. \quad (22)$$

Then for $x \in H \setminus N_1$, $(x, T^*(x)) \in H \times H \setminus N$, thus,

$$(V^*)^c(x) + V^*(T^*(x)) = c(x, T^*(x)). \quad (23)$$

Therefore,

$$T^*(x) \in \arg \min_{y \in H} [c(x, y) - V^*(y)] \quad (24)$$

for μ -almost surely $x \in H$.

C.2. Proof of Theorem 3.2 (1)

Lemma C.2. *Let $f : H \rightarrow \mathbb{R}$ be a locally bounded convex function. Then f is locally Lipschitz continuous.*

Proof. Let $x_0 \in H$ and $r > 0$ be such that $|f(u)| \leq M$ for all $u \in B_{2r}(x_0)$. Let $x, y \in B_r(x_0)$ be two distinct points. Define a point z extending the segment from x through y to the boundary of the ball of radius r centered at x :

$$z := x + \frac{r}{\|x - y\|_H} (y - x).$$

Then $\|z - x\|_H = r$, and by the triangle inequality, $\|z - x_0\|_H \leq \|z - x\|_H + \|x - x_0\|_H < r + r = 2r$, so $z \in B_{2r}(x_0)$. Since y lies on the segment connecting x and z , we can write $y = (1 - \lambda)x + \lambda z$ with $\lambda = \frac{\|y - x\|_H}{r} \in (0, 1)$. By the convexity of f ,

$$f(y) \leq (1 - \lambda)f(x) + \lambda f(z) = f(x) + \lambda(f(z) - f(x)).$$

Rearranging the terms yields:

$$f(y) - f(x) \leq \lambda(f(z) - f(x)) \leq \lambda(|f(z)| + |f(x)|) \leq \frac{\|x - y\|_H}{r}(2M).$$

Interchanging the roles of x and y , we similarly obtain:

$$f(x) - f(y) \leq \frac{2M}{r}\|x - y\|_H.$$

Combining these two inequalities, we conclude:

$$|f(y) - f(x)| \leq \frac{2M}{r}\|x - y\|_H.$$

Thus, f is Lipschitz continuous on $B_r(x_0)$ with the constant $L = 2M/r$. \square

Step 1. Gâteaux differentiability of V^ .*

Since V^* is the maximal Kantorovich potential, V^* satisfies

$$\begin{aligned} V^*(x) &= \inf_{y \in H} \left[\frac{1}{2}\|x - y\|_H^2 - (V^*)^c(y) \right] \\ &= \inf_{y \in H} \left[\frac{1}{2}\|x\|_H^2 - \langle x, y \rangle_H + \frac{1}{2}\|y\|_H^2 - (V^*)^c(y) \right] \\ &= \frac{1}{2}\|x\|_H^2 - \sup_{y \in H} \left[\langle x, y \rangle_H - \left[\frac{1}{2}\|y\|_H^2 + (V^*)^c(y) \right] \right]. \end{aligned}$$

Let us define the function $\varphi : H \rightarrow \mathbb{R} \cup \{+\infty\}$ as

$$\varphi(x) := \sup_{y \in H} [\langle x, y \rangle_H - \zeta(y)], \quad \text{where } \zeta(y) := \frac{1}{2}\|y\|_H^2 + (V^*)^c(y).$$

Then $V^*(x) = \frac{1}{2}\|x\|_H^2 - \varphi(x)$. Since $x \mapsto \langle x, y \rangle_H - \zeta(y)$ is affine and continuous, φ is convex and lower semi-continuous.

Since $V^* \in L^1(H, \nu)$, we have $|V^*| < \infty$ ν -almost surely. This implies that φ is also finite ν -almost surely. Moreover, if x, y are points where φ is finite, then by the convexity of φ , it is finite on the line segment connecting x and y . Thus, φ is finite on the convex hull of $\text{supp}(\nu)$.

By Lemma C.2, φ is locally Lipschitz continuous on this convex hull, and thus V^* is also locally Lipschitz. By the infinite-dimensional Rademacher theorem (Ambrosio et al., 2005, Theorem 6.2.3), V^* is Gâteaux differentiable except on Gaussian null sets.

Step 2. Uniqueness of the minimizer.

Suppose that $(x, y) \in H \times H$ satisfies

$$V^*(x) + (V^*)^c(y) = c(x, y). \tag{25}$$

Since $V^*(z) + (V^*)^c(y) \leq c(z, y)$ for all $z \in H$, the nonnegative function

$$G(z) := c(z, y) - (V^*)^c(y) - V^*(z)$$

achieves a global minimum at $z = x$. Thus, the Gâteaux differential at x satisfies

$$0 = \nabla G(x) = \nabla_x c(x, y) - \nabla V^*(x).$$

Hence

$$\nabla V^*(x) = \nabla_x c(x, y) = x - y. \quad (26)$$

If y_1, y_2 both satisfy (Eq. 25) for same x , then

$$x - y_1 = \nabla V^*(x) = x - y_2,$$

so $y_1 = y_2$. Thus for μ -a.e. $x \in H$, there exists a unique $y \in H$ satisfying (Eq. 25). Due to (Eq. 24), we obtain the desired result.

C.3. Proof of Theorem 3.2 (2)

1. First, we prove that T^* is a minimizer. By the definition of the c -transform, for any $x \in H$,

$$(V^*)^c(x) = \inf_{y \in H} [c(x, y) - V^*(y)].$$

Therefore, for any measurable map $T : H \rightarrow H$, the following pointwise inequality holds:

$$c(x, T(x)) - V^*(T(x)) \geq (V^*)^c(x).$$

Integrating both sides with respect to μ yields a lower bound for the objective function:

$$\begin{aligned} \mathcal{L}(V^*, T) &= \int_H (c(x, T(x)) - V^*(T(x))) \mu(dx) + \int_H V^*(y) \nu(dy) \\ &\geq \int_H (V^*)^c(x) \mu(dx) + \int_H V^*(y) \nu(dy) = S(\mu, \nu). \end{aligned} \quad (27)$$

Thus,

$$\inf_{T: H \rightarrow H} \mathcal{L}(V^*, T) \geq S(\mu, \nu).$$

Now, consider the Monge map T^* . By (Eq. 23), the equality holds μ -almost surely:

$$c(x, T^*(x)) - V^*(T^*(x)) = (V^*)^c(x), \quad \mu\text{-a.e.}$$

Substituting this into the objective function:

$$\mathcal{L}(V^*, T^*) = \int_H (V^*)^c(x) \mu(dx) + \int_H V^*(y) \nu(dy) = S(\mu, \nu).$$

Since $\mathcal{L}(V^*, T^*)$ attains the lower bound, T^* is a minimizer.

Now, we prove the uniqueness of the minimizer. Assume that there exists another minimizer $\bar{T} : H \rightarrow H$. Since \bar{T} achieves the lower bound in (Eq. 27), we have:

$$\int_H (c(x, \bar{T}(x)) - V^*(\bar{T}(x))) \mu(dx) = \int_H (V^*)^c(x) \mu(dx).$$

Rearranging the terms, we get:

$$\int_H \underbrace{(c(x, \bar{T}(x)) - V^*(\bar{T}(x)) - (V^*)^c(x))}_{\geq 0} \mu(dx) = 0.$$

Since the integrand is non-negative by definition of the c -transform, the integral being zero implies that the integrand must be zero μ -almost everywhere. That is, for μ -almost every x :

$$c(x, \bar{T}(x)) - V^*(\bar{T}(x)) = (V^*)^c(x) = \inf_{y \in H} [c(x, y) - V^*(y)].$$

This implies:

$$\bar{T}(x) \in \arg \min_{y \in H} [c(x, y) - V^*(y)] := \mathcal{D}_x.$$

Since $\mu \in \mathcal{P}_2^r(H)$ (the source measure is regular), Theorem 3.2 guarantees that the set \mathcal{D}_x is a singleton for μ -almost every x , specifically $\mathcal{D}_x = \{T^*(x)\}$. Therefore, $\bar{T}(x) = T^*(x)$ for μ -almost every x . Hence, the minimizer is unique.

2. From the Inner Minimization condition in (Eq. 36), $(\inf_T \mathcal{L}(V^*, T) = \mathcal{L}(V^*, T^*))$, T^* must minimize the integrand pointwise. Specifically, for μ -almost every x :

$$c(x, T^*(x)) - V^*(T^*(x)) = \inf_{y \in H} [c(x, y) - V^*(y)] = (V^*)^c(x).$$

This implies that for a pair (V^*, T^*) satisfying (Eq. 36),

$$\begin{aligned} \mathcal{L}(V^*, T^*) &= \int_H [c(x, T^*(x)) - V^*(T^*(x))] \mu(dx) + \int_H V^*(y) \nu(dy) \\ &= \int_H (V^*)^c(x) \mu(dx) + \int_H V^*(y) \nu(dy) =: J(V^*), \end{aligned} \quad (28)$$

where $J(V)$ is the standard Kantorovich dual functional.

On the other hand, since T^* is the Monge map, it satisfies the push-forward constraint $T^*_\# \mu = \nu$. As discussed before,

$$\begin{aligned} \mathcal{L}(V^*, T^*) &= \int_H c(x, T^*(x)) \mu(dx) - \underbrace{\left(\int_H V^*(T^*(x)) \mu(dx) - \int_H V^*(y) \nu(dy) \right)}_{=0} \\ &= \int_H c(x, T^*(x)) \mu(dx) = \text{Primal Cost}. \end{aligned} \quad (29)$$

Combining (Eq. 28) and (Eq. 29),

$$J(V^*) = \int_H (V^*)^c(x) \mu(dx) + \int_H V^*(y) \nu(dy) = \text{Primal Cost}.$$

By the Kantorovich Duality Theorem, a potential V is optimal (*i.e.*, a Kantorovich potential) if and only if its dual objective value equals the primal cost. Therefore, V^* is a Kantorovich potential.

D. Proof of Theorem 4.3

Lemma D.1. *Let H be a separable Hilbert space and $\{e_k\}_{k \in \mathbb{N}}$ an orthonormal basis of H .*

1. *If $\{\lambda_k\}_{k \in \mathbb{N}} \subset [0, \infty)$ is summable, then*

$$Qx := \sum_{k=1}^{\infty} \lambda_k \langle x, e_k \rangle_H e_k, \quad x \in H, \quad (30)$$

defines a covariance operator with $\text{tr } Q = \sum_k \lambda_k$. Conversely, if Q is a covariance operator, then there exists a summable sequence $\{\lambda_k\} \subset [0, \infty)$ with $Qe_k = \lambda_k e_k$, hence (Eq. 30) holds.

2. *For $\alpha \in [0, \infty)$ and a covariance operator Q which satisfies (Eq. 30), the fractional operator*

$$Q^\alpha x := \sum_{k=1}^{\infty} \lambda_k^\alpha \langle x, e_k \rangle_H e_k$$

is a self-adjoint, positive, bounded, and linear operator. If $\sum_{k=1}^{\infty} \lambda_k^\alpha < \infty$, then Q^α is also a covariance operator.

3. *The Hilbert space H has an orthogonal decomposition with respect to a trace-class operator Q :*

$$\begin{aligned} H &= \overline{\text{Ran}(Q^\alpha)} \oplus \text{Ker}(Q) \\ &:= \{x + y : x \in \overline{\text{Ran}(Q^\alpha)}, y \in \text{Ker}(Q)\}, \end{aligned} \quad (31)$$

where $\alpha \in (0, 1)$,

$$\text{Ran}(Q^\alpha) := \{x \in H : \exists y \in H \text{ such that } x = Q^\alpha y\}, \quad \text{and} \quad \text{Ker}(Q) := \{x \in H : Qx = 0\}.$$

Proof. 1. Since $\langle Qe_k, e_k \rangle_H = \lambda_k$ and $\{\lambda_k\}_{k \in \mathbb{N}}$ is summable, Q is a trace-class operator. For the converse direction, it is straightforward by defining $\lambda_k := \langle Qe_k, e_k \rangle_H$.

2. Boundedness is immediate since $\|Q^\alpha\| \leq \sup_k \lambda_k^\alpha$. Trace-class is also obtained from $\text{tr}(Q^\alpha) = \sum_k \lambda_k^\alpha$.

3. From $Qe_k = \lambda_k e_k$ we have

$$\text{Ker}(Q) = \text{span}\{e_k : \lambda_k = 0\} = \text{Ker}(Q^\alpha).$$

Since $\{0\} \subset H$ is closed,

$$\text{Ker}(Q^\alpha) = Q^{-\alpha}(\{0\})$$

is also closed, and is also a subspace because Q is bounded and linear. Due to (Conway, 2019, Theorem 2.19),

$$\text{Ker}(Q^\alpha)^\perp = \overline{\text{Ran}(Q^\alpha)}.$$

By (Rudin, 1987, Theorem 4.11), we obtain the result. \square

Remark D.2. 1. In (Eq. 31), the closure of the space

$$H_Q := \text{Ran}(Q^{1/2}) = \text{Dom}(Q^{-1/2}) = \left\{ x \in H : \sum_{k: \lambda_k > 0} \frac{\langle x, e_k \rangle_H^2}{\lambda_k} < \infty, \langle x, e_k \rangle_H = 0 \text{ if } \lambda_k = 0 \right\}$$

is a *Cameron-Martin space* which is a Hilbert space with the inner product by

$$\langle x, y \rangle_Q := \langle Q^{-1/2}x, Q^{-1/2}y \rangle_H.$$

Theorem D.3. Let μ be a centered Gaussian measure with a covariance operator Q on H . Then

1. $\mu(\overline{H_Q}) = 1$.
2. $\mu(H_Q) = 0$ if $\dim(H_Q) = \infty$.
3. $\mu(H_Q) = 1$ if $\dim(H_Q) < \infty$.

Proof. Let X be a H -valued Gaussian random vector defined in (Eq. 19). By Proposition 4.4, $\mu = \text{Law}(X) = \mathcal{N}(0, Q)$.

1. Since $\langle X, h \rangle_H \sim \mathcal{N}(\langle m, h \rangle_H, \langle Qh, h \rangle_H)$, for $h \in \text{Ker}(Q)$, $\mathbb{E}[\langle X, h \rangle_H^2] = \langle Qh, h \rangle_H = 0$. By Chebyshev's inequality

$$\mathbb{P}(|\langle X, h \rangle_H| > \varepsilon) \leq \frac{\mathbb{E}[|\langle X, h \rangle_H|^2]}{\varepsilon^2} = 0$$

for all $\varepsilon > 0$. Therefore, $\langle X, h \rangle_H = 0$ almost surely, and $X \in \text{Ker}(Q)^\perp$ almost surely, thus

$$\mu(\overline{H_Q}) = 1.$$

2. By the definition of H_Q and X ,

$$X \in H_Q \iff \sum_{k: \lambda_k > 0} \frac{\langle X, e_k \rangle_H^2}{\lambda_k} = \sum_{k: \lambda_k > 0} \xi_k^2 < \infty.$$

One can directly check that

$$\dim(H_Q) = \#\{k \text{ such that } \lambda_k > 0\}.$$

Since $\dim(H_Q) = \infty$ and $\xi_k^2 \sim \chi^2(1)$ are independent and identically distributed random variables, the law of large numbers yields

$$\lim_{n \rightarrow \infty} \frac{1}{n} \sum_{k \in D_n} \xi_k^2 = 1$$

almost surely, where

$$D_1 \subseteq D_2 \subseteq \dots \subseteq D_n \subseteq \dots \subseteq \{k \in \mathbb{N} : \lambda_k > 0\}, \quad |D_n| = n.$$

Therefore, $\sum_{k:\lambda_k>0} \xi_k^2 = \infty$ almost surely, and this implies that $\mathbb{P}(X \in H_Q) = \mu(H_Q) = 0$.

3. If $\dim(H_Q) = n < \infty$, then

$$\mathbb{E} \left[\sum_{k:\lambda_k>0} \xi_k^2 \right] = n$$

By Chebyshev's inequality,

$$\mathbb{P} \left(\sum_{k:\lambda_k>0} \xi_k^2 = \infty \right) = \lim_{\lambda \rightarrow \infty} \mathbb{P} \left(\sum_{k:\lambda_k>0} \xi_k^2 > \lambda \right) \leq \lim_{\lambda \rightarrow \infty} \frac{n}{\lambda} = 0.$$

Therefore, $\mathbb{P}(X \in H_Q) = \mu(H_Q) = 1$. \square

Theorem D.4 (Cameron-Martin theorem). *Let μ be a centered Gaussian measure with a covariance operator Q . Then μ_h is absolutely continuous with respect to μ if and only if $h \in \overline{H_Q}$, where*

$$\mu_h(A) := \mu(A - h), \quad A - h := \{x - h : x \in A\}.$$

Proof. See (Hairer, 2009, Theorem 4.4). \square

Lemma D.5. *Let μ be a centered nondegenerate Gaussian measure on H . Then for every $\nu \in \mathcal{P}(H)$, the convolution $\mu * \nu$ belongs to $\mathcal{P}^r(H)$.*

Proof. Let $X \sim \mathcal{N}(0, Q)$ so that $\text{Law}(X) = \mu$. For each $x \in H$, consider the translated random variable $Y := X + x$. Its characteristic function satisfies

$$\mathbb{E}[e^{i\langle Y, h \rangle_H}] = e^{i\langle x, h \rangle_H} \exp\left(-\frac{1}{2}\langle Qh, h \rangle_H\right), \quad h \in H,$$

hence

$$\text{Law}(Y) =: \mu_x = \mathcal{N}(x, Q).$$

Thus, μ_x is a nondegenerate Gaussian measure for every $x \in H$. In particular, if $B \subset H$ is a Gaussian null set, then by definition

$$\mu_x(B) = 0 \quad \text{for all } x \in H.$$

Now, let B be a Gaussian null set in H . Using the definition of convolution,

$$(\mu * \nu)(B) = \int_H \mu(B - x) \nu(dx) = \int_H \mu_x(B) \nu(dx) = 0.$$

Hence, $\mu * \nu$ assigns zero measure to every Gaussian null set, so $\mu * \nu \in \mathcal{P}^r(H)$. \square

Let

$$T : (h, k) \in \overline{H_Q} \times \text{Ker}(Q) \mapsto h + k \in H, \quad T^{-1} : h \in H \mapsto (\pi_Q h, \pi_K h) \in \overline{H_Q} \times \text{Ker}(Q),$$

where $\pi_Q : H \rightarrow \overline{H_Q}$ and $\pi_K : H \rightarrow \text{Ker}(Q)$ are projections. Then T is an unitary map.

Lemma D.6. *Let γ be a centered Gaussian measure with a covariance operator Q . For $\mu \in \mathcal{P}(H)$, set*

$$\tilde{\mu} := T_{\#}^{-1} \mu, \quad \mu_K := (\text{pr}_2)_{\#} \tilde{\mu} = (\pi_K)_{\#} \mu,$$

where $\text{pr}_2 : (h, k) \in \overline{H_Q} \times \text{Ker}(Q) \mapsto k$. Let $\rho := \gamma * \mu$ and $\rho' := T_{\#}^{-1} \rho$. Then for μ_K -almost every $k \in \text{Ker}(Q)$, there exists a family $\mu_k \in \mathcal{P}(\overline{H_Q})$ such that

$$\tilde{\mu}(dh, dk) = \mu_k(dh) \mu_K(dk).$$

Moreover, ρ' admits the disintegration

$$\rho'(dh, dk) = \rho'_k(dh) \mu_K(dk), \quad \text{for } \mu_K\text{-almost every } k \in K,$$

and for such k ,

$$\rho'_k = \gamma_Q * \mu_k, \quad \gamma_Q := (\pi_Q)_{\#} \gamma.$$

Proof. Let $(\Omega, \mathcal{F}, \mathbb{P})$ be a probability space, and let $X, Z : \Omega \rightarrow H$ be independent random vectors such that

$$\text{Law}(X) = \gamma = \mathcal{N}(0, Q), \quad \text{Law}(Z) = \mu.$$

Recall the orthogonal decomposition $H = \overline{H_Q} \oplus \text{Ker}(Q)$ and the unitary map $T : (h, k) \overline{H_Q} \times \text{Ker}(Q) \mapsto h + k \in H$. We write

$$(Y, \tilde{Y}) := T^{-1}(X) = (\pi_Q X, \pi_K X), \quad (Z_Q, Z_K) := T^{-1}(Z) = (\pi_Q Z, \pi_K Z),$$

so that $X = Y + \tilde{Y}$ and $Z = Z_Q + Z_K$.

By Theorem D.3, we know that $\pi_K X = 0$ almost surely, *i.e.*, $\tilde{Y} = 0$ a.s., hence $X = Y$ a.s. with $Y \in \overline{H_Q}$. In particular, $\text{Law}(Y) = \mu_Q$ is a nondegenerate Gaussian measure on $\overline{H_Q}$.

Define

$$W := X + Z, \quad (W_Q, W_K) := T^{-1}(W) = (\pi_Q W, \pi_K W).$$

Using $X = Y$ a.s. and $Z = Z_Q + Z_K$, we have

$$W = X + Z = Y + Z_Q + Z_K,$$

and therefore

$$(W_Q, W_K) = (\pi_Q W, \pi_K W) = (Y + Z_Q, Z_K).$$

Thus $\rho' = T_{\#}^{-1}\rho = \text{Law}(W_Q, W_K)$, and its $\text{Ker}(Q)$ -marginal is

$$(\text{pr}_2)_{\#}\rho' = \text{Law}(W_K) = \text{Law}(Z_K) = \mu_K.$$

Next we apply the disintegration theorem to the joint law of (Z_Q, Z_K) . By (Ambrosio et al., 2005, Theorem 5.3.1), there exists a μ_K -measurable family $\{\mu_k\}_{k \in \text{Ker}(Q)}$ of probability measures on $\overline{H_Q}$ such that

$$\text{Law}(Z_Q, Z_K) = \mu_k(dh)\mu_K(dk),$$

that is,

$$\mathbb{P}(Z_Q \in E, Z_K \in B) = \int_B \mu_k(E) \mu_K(dk)$$

for all Borel sets $E \subset \overline{H_Q}$ and $B \subset \text{Ker}(Q)$. Equivalently, for μ_K -almost every k ,

$$\mu_k(\cdot) = \mathbb{P}(Z_Q \in \cdot \mid Z_K = k),$$

so ν_k is the conditional law of Z_Q given $Z_K = k$.

We now compute the conditional law of W_Q given W_K . Let $\varphi : H_Q \rightarrow \mathbb{R}$ be a bounded Borel function. For any bounded Borel function $\psi : K \rightarrow \mathbb{R}$ we have

$$\int_{\overline{H_Q} \times \text{Ker}(Q)} \varphi(h) \psi(k) \rho'(dh, dk) = \mathbb{E}[\varphi(W_Q) \psi(W_K)] = \mathbb{E}[\varphi(Y + Z_Q) \psi(Z_K)].$$

Using the independence of Y and (Z_Q, Z_K) , and $\text{Law}(Y) = \gamma_Q$, we obtain

$$\begin{aligned} \mathbb{E}[\varphi(Y + Z_Q) \psi(Z_K)] &= \mathbb{E}\left[\psi(Z_K) \mathbb{E}[\varphi(Y + Z_Q) \mid Z_Q, Z_K]\right] \\ &= \mathbb{E}\left[\psi(Z_K) \int_{\overline{H_Q}} \varphi(y + Z_Q) \gamma_Q(dy)\right], \end{aligned}$$

Using again the disintegration of $\text{Law}(Z_Q, Z_K)$, this equals

$$\int_{\text{Ker}(Q)} \psi(k) \left(\int_{\overline{H_Q}} \int_{\overline{H_Q}} \varphi(y + z) \gamma_Q(dy) \mu_k(dz) \right) \mu_K(dk).$$

We now recognize the inner integral as the convolution of γ_Q and μ_k :

$$\int_{\overline{H_Q}} \int_{\overline{H_Q}} \varphi(y+z) \gamma_Q(dy) \mu_k(dz) = \int_{\overline{H_Q}} \varphi(h) (\gamma_Q * \mu_k)(dh).$$

Therefore

$$\int_{\overline{H_Q} \times \text{Ker}(Q)} \varphi(h) \psi(k) \rho'(dh, dk) = \int_{\text{Ker}(Q)} \psi(k) \left(\int_{\overline{H_Q}} \varphi(h) (\gamma_Q * \mu_k)(dh) \right) \mu_K(dk).$$

On the other hand, if we disintegrate ρ' with respect to its second marginal ν_K , there exists a family $\{\rho'_k\}_{k \in \text{Ker}(Q)}$ of probability measures on $\overline{H_Q}$ such that

$$\rho'(dh, dk) = \rho'_k(dh) \nu_K(dk),$$

and hence

$$\int_{\overline{H_Q} \times \text{Ker}(Q)} \varphi(h) \psi(k) \rho'(dh, dk) = \int_{\text{Ker}(Q)} \psi(k) \left(\int_{\overline{H_Q}} \varphi(h) \rho'_k(dh) \right) \mu_K(dk).$$

Comparing the two identities for all bounded Borel φ and ψ , we obtain

$$\int_{\overline{H_Q}} \varphi(h) \rho'_k(dh) = \int_{\overline{H_Q}} \varphi(h) (\gamma_Q * \mu_k)(dh)$$

for μ_K -almost every $k \in K$ and all bounded Borel φ . Therefore

$$\rho'_k = \gamma_Q * \mu_k \quad \text{for } \mu_K\text{-a.e. } k \in \text{Ker}(Q),$$

which is the desired identity. \square

Proof of Theorem 4.3. First, we show that $\mu_K \in \mathcal{P}^r(\text{Ker}(Q))$ whenever $\gamma * \mu \in \mathcal{P}^r(H)$. Let $B \subset \text{Ker}(Q)$ be a Gaussian null set, and define

$$A := \overline{H_Q} \oplus B.$$

Step 1. A is a Gaussian null set in H .

Let $Y \sim \mathcal{N}(m, C)$, where C is a nondegenerate trace-class operator on H , and denote its law by Γ . We claim that

$$\Gamma(A) = 0.$$

Consider the projection $Z := \pi_K Y$. By definition of the push-forward measure, $\Gamma_K := (\pi_K)_\# \Gamma$ is the law of Y on $\text{Ker}(Q)$. For any $k \in \text{Ker}(Q)$,

$$\mathbb{E}[e^{i\langle Z, k \rangle_{\text{Ker}(Q)}}] := \mathbb{E}[e^{i\langle Z, k \rangle_H}] = \mathbb{E}[e^{i\langle \pi_K Y, k \rangle_H}] = \mathbb{E}[e^{i\langle Y, k \rangle_H}] = \exp \left(i\langle m, k \rangle_H - \frac{\langle Ck, k \rangle_H}{2} \right).$$

Hence $Z \sim \mathcal{N}(\pi_K m, C_K)$ on $\text{Ker}(Q)$, where $C_K := (\pi_K C)|_{\text{Ker}(Q)} : \text{Ker}(Q) \rightarrow \text{Ker}(Q)$. To check that Γ_K is nondegenerate, let $k \neq 0$ in $\text{Ker}(Q)$. Since C is nondegenerate on H ,

$$\langle C_K k, k \rangle_H = \langle Ck, k \rangle_H > 0.$$

Thus Γ_K is a nondegenerate Gaussian measure on $\text{Ker}(Q)$. Since B is Gaussian null set in $\text{Ker}(Q)$ and Γ_K is a nondegenerate Gaussian measure on $\text{Ker}(Q)$,

$$\Gamma(A) = \Gamma(\pi_K^{-1}(B)) = \Gamma_K(B) = 0.$$

Step 2. $(\gamma * \mu)(A) = \mu_K(B)$.

Let

$$T : (h, k) \in \overline{H_Q} \times \text{Ker}(Q) \mapsto h + k \in H, \quad T^{-1} : x \in H \mapsto (\pi_Q x, \pi_K x) \in \overline{H_Q} \times \text{Ker}(Q).$$

By Theorem D.3, $X = \pi_Q X$ almost surely, thus $\pi_K X = 0$ almost surely. This implies that for $A \subseteq \overline{H_Q}$ and $B \subseteq \text{Ker}(Q)$,

$$T_{\#}\mu(A \times B) = \mathbb{P}(\pi_Q X \in A, \pi_K X \in B) = \mathbb{P}(X \in A, 0 \in B) = \mathbb{P}(X \in A) \delta_0(B) = \gamma(A) \delta_0(B).$$

Therefore,

$$\begin{aligned} (\mu * \nu)(A) &= \int_H \gamma(A - x) \mu(dx) \\ &= \int_H \gamma(T(\overline{H_Q} \times B) - T(\pi_Q x, \pi_K x)) \mu(dx) \\ &= \int_H \gamma(T(\overline{H_Q} \times (B - \pi_K x))) \mu(dx) \\ &= \int_H T_{\#} \gamma(\overline{H_Q} \times (B - \pi_K x)) \mu(dx) \\ &= \gamma(\overline{H_Q}) \int_H \delta_0(B - \pi_K x) \mu(dx) = \gamma(\overline{H_Q}) \mu_K(B). \end{aligned}$$

By Theorem D.3, $\gamma(\overline{H_Q}) = 1$.

Now we prove the converse, $\gamma * \mu \in \mathcal{P}^r(H)$ whenever $\mu_K \in \mathcal{P}^r(\text{Ker}(Q))$.

Step 3. For a Gaussian null set $A \subset H$,

$$N := \{k \in \text{Ker}(Q) : \rho'_k(A'_k) > 0\} \quad (32)$$

is a Gaussian null set in $\text{Ker}(Q)$. Here $A'_k := \{h \in \overline{H_Q} : (h, k) \in T^{-1}(A)\}$.

Let Γ_K be a nondegenerate Gaussian measure on $\text{Ker}(Q)$. Then $\gamma_Q \otimes \Gamma_K$ is a nondegenerate Gaussian measure on $\overline{H_Q} \times \text{Ker}(Q)$, and

$$\Gamma := T_{\#}(\gamma_Q \otimes \Gamma_K)$$

is a nondegenerate Gaussian measure on H . Since A is a Gaussian null set in H ,

$$0 = \Gamma(A) = (\gamma_Q \otimes \Gamma_K)(T^{-1}(A)).$$

By Fubini's theorem

$$\begin{aligned} (\gamma_Q \otimes \Gamma_K)(T^{-1}(A)) &= \int_{\overline{H_Q} \times \text{Ker}(Q)} 1_{T^{-1}(A)}(h, k) (\gamma_Q \otimes \Gamma_K)(dh, dk) \\ &= \int_{\text{Ker}(Q)} \int_{\overline{H_Q}} 1_{T^{-1}(A)}(h, k) \gamma_Q(dh) \Gamma_K(dk) = \int_{\text{Ker}(Q)} \gamma_Q(A'_k) \Gamma_K(dk). \end{aligned}$$

Therefore, $\gamma_Q(A'_k) = 0$ for Γ_K -a.e. $k \in \text{Ker}(Q)$. By the Cameron-Martin theorem (Theorem D.4), $\gamma_Q(A'_k - h) = 0$ for all $h \in \overline{H_Q}$, thus

$$\rho'_k(A'_k) = \int_{\overline{H_Q}} \gamma_Q(A'_k - h) \mu_k(dh) = 0$$

for Γ_K -a.e. $k \in \text{Ker}(Q)$. This also implies that $\Gamma_K(N) = 0$. Since Γ_K is arbitrary nondegenerate Gaussian measure on $\text{Ker}(Q)$, N is a Gaussian null set in $\text{Ker}(Q)$.

Step 4. $(\gamma * \mu)(A) = 0$ for a Gaussian null set $A \subset H$.

By the disintegration theorem (Lemma D.6),

$$(\gamma * \mu)(A) = T_{\#}^{-1}(\gamma * \mu)(T^{-1}(A)) = \int_{\text{Ker}(Q)} \rho'_k(A'_k) \mu_K(dk),$$

where $\rho'_k = \gamma_Q * \mu_k$. Since $\mu_K \in \mathcal{P}^r(\text{Ker}(Q))$, by Step 3, $\mu_K(N) = 0$ and $\rho'_k(A'_k) = 0$ for $k \in \text{Ker}(Q) \setminus N$, where N is the set in (Eq. 32). Therefore,

$$\int_{\text{Ker}(Q)} \rho'_k(A'_k) \mu_K(dk) = \int_{\text{Ker}(Q) \setminus N} \rho'_k(A'_k) \mu_K(dk) + \int_N \rho'_k(A'_k) \mu_K(dk) = 0$$

This completes the proof. \square

E. Convergence of OTP

Proof of Theorem 4.2. Since $\mu_k \in \mathcal{P}_2^r(H)$, by Proposition C.1, the optimal transport plan is given by $\pi_k^* = (Id \times T_k^*)\# \mu_k$. Since μ_k converges to μ in $\mathcal{P}_2(H)$, the second moments converge, *i.e.*, $\int_H \|x\|_H^2 \mu_k(dx) \rightarrow \int_H \|x\|_H^2 \mu(dx)$. Using the inequality $\|x - y\|_H^2 \leq 2(\|x\|_H^2 + \|y\|_H^2)$, we have

$$\begin{aligned} \liminf_{k \rightarrow \infty} \iint_{H \times H} \|x - y\|_H^2 \pi_k^*(dx, dy) &\leq \liminf_{k \rightarrow \infty} 2 \left(\int_H \|x\|_H^2 \mu_k(dx) + \int_H \|y\|_H^2 \nu(dy) \right) \\ &= 2 \left(\int_H \|x\|_H^2 \mu(dx) + \int_H \|y\|_H^2 \nu(dy) \right) < \infty. \end{aligned}$$

Thus, both assumptions (consistency of plans and finiteness of costs) in (Villani et al., 2009, Theorem 5.20) are satisfied, and the desired result is obtained. \square

To apply Theorem 4.2 to our framework, specifically for the Gaussian smoothing approximations, we rely on the following lemma which guarantees the required convergence in the Wasserstein metric.

Lemma E.1. *Let $\mu \in \mathcal{P}_2(H)$, and let γ be a centered Gaussian measure with covariance operator Q . Then, the convolution $\gamma_\epsilon * \mu$ converges to μ in the Wasserstein metric W_2 as $\epsilon \rightarrow 0$. Here, γ_ϵ denotes a centered Gaussian measure with covariance operator ϵQ .*

Proof. Let X and Y_ϵ be independent H -valued random vectors satisfying

$$\text{Law}(X) = \mu, \quad \text{Law}(Y_\epsilon) = \gamma_\epsilon.$$

Then, the sum $X + Y_\epsilon$ follows the distribution $\gamma_\epsilon * \mu$. Since γ_ϵ is a centered Gaussian measure with covariance ϵQ , we have

$$\lim_{\epsilon \rightarrow 0} \mathbb{E}[\|(X + Y_\epsilon) - X\|_H^2] = \lim_{\epsilon \rightarrow 0} \mathbb{E}[\|Y_\epsilon\|_H^2] = \lim_{\epsilon \rightarrow 0} \epsilon \text{Tr}(Q) = 0.$$

This implies that $X + Y_\epsilon$ converges to X in $L^2(\Omega)$. Since convergence in $L^2(\Omega)$ implies convergence in the Wasserstein W_2 distance for the induced laws, we conclude that $\gamma_\epsilon * \mu$ converges to μ in $\mathcal{P}_2(H)$. \square

F. Gaussian Smoothing in Hilbert Spaces

In this section, we provide the theoretical justification for the Gaussian random field construction used in our spectral augmentation strategy, followed by specific examples of orthonormal bases implemented in our experiments.

F.1. Proof of Proposition 4.4

Here we prove that the series defined in the main text converges to a valid Gaussian random variable in H .

Proof. Let $X_N := \sum_{k=1}^N \sqrt{\lambda_k} \xi_k e_k$ be the partial sum. We first show that $\{X_N\}_{N \in \mathbb{N}}$ is a Cauchy sequence in $L^2(\Omega; H)$. For $M > N$, we have:

$$\begin{aligned} \mathbb{E}[\|X_M - X_N\|_H^2] &= \mathbb{E} \left[\left\| \sum_{k=N+1}^M \sqrt{\lambda_k} \xi_k e_k \right\|_H^2 \right] \\ &= \sum_{k=N+1}^M \lambda_k \mathbb{E}[\xi_k^2] \|e_k\|_H^2 \\ &= \sum_{k=N+1}^M \lambda_k. \end{aligned}$$

Since $\{\lambda_k\}_{k \in \mathbb{N}}$ is summable (trace-class condition), the tail sum converges to 0 as $N, M \rightarrow \infty$. Thus, X_N converges to a limit X in $L^2(\Omega; H)$. By the Itô-Nisio theorem, this implies that X converges almost surely in H .

To verify that X is Gaussian, consider an arbitrary linear functional $\ell(h) = \langle h, u \rangle_H$ for $u \in H$. Then

$$\langle X, u \rangle_H = \sum_{k=1}^{\infty} \sqrt{\lambda_k} \xi_k \langle e_k, u \rangle_H.$$

This is a countable sum of independent Gaussian random variables. Since the variance

$$\sum_{k=1}^{\infty} \lambda_k \langle e_k, u \rangle^2 \leq \left(\max_{k \in \mathbb{N}} \lambda_k \right) \|u\|_H^2 < \infty,$$

the limit is a univariate Gaussian random variable. Thus, X is a Gaussian random vector.

Finally, we identify the covariance operator Q . For any $u, v \in H$,

$$\begin{aligned} \mathbb{E}[\langle X, u \rangle \langle X, v \rangle] &= \mathbb{E} \left[\left(\sum_{j=1}^{\infty} \sqrt{\lambda_j} \xi_j \langle e_j, u \rangle \right) \left(\sum_{k=1}^{\infty} \sqrt{\lambda_k} \xi_k \langle e_k, v \rangle \right) \right] \\ &= \sum_{j,k=1}^{\infty} \sqrt{\lambda_j \lambda_k} \delta_{jk} \langle e_j, u \rangle \langle e_k, v \rangle \\ &= \sum_{k=1}^{\infty} \lambda_k \langle e_k, u \rangle \langle e_k, v \rangle \\ &= \langle Qu, v \rangle, \end{aligned}$$

where Q is the operator defined by $Qe_k = \lambda_k e_k$. This completes the proof. \square

F.2. Examples of Orthonormal Bases

As described in the **Practical Smoothing via Spectral Augmentation** section, our method projects data onto an orthonormal basis $\{e_k\}$ to inject noise. In our experiments, we specifically utilized the Fourier basis. We detail this basis below, along with other illustrative examples for $H = L^2(-1, 1)$ that are compatible with our framework.

1. Fourier Basis. On the interval $(-1, 1)$, the orthonormal basis is defined as:

$$e_k(t) = \begin{cases} \frac{1}{\sqrt{2}} & \text{if } k = 0, \\ \cos(m\pi t) & \text{if } k = 2m, \\ \sin(m\pi t) & \text{if } k = 2m - 1. \end{cases}$$

2. Legendre Polynomials. Let $P_n(t)$ be the Legendre polynomials satisfying the recurrence relation $(n+1)P_{n+1}(t) = (2n+1)tP_n(t) - nP_{n-1}(t)$ with $P_0(t) = 1, P_1(t) = t$. To ensure orthonormality on $L^2(-1, 1)$, we apply the normalization factor $\sqrt{\frac{2k+1}{2}}$:

$$e_k(t) = \sqrt{\frac{2k+1}{2}} P_k(t), \quad k \in \mathbb{N}_0.$$

This basis is particularly useful for capturing global trends without enforcing periodicity at the boundaries.

3. Haar Wavelets. Let $h_0(t) = \frac{1}{\sqrt{2}} \mathbf{1}_{(-1,1)}(t)$. For scale $j \in \mathbb{N}_0$ and shift $k = 0, \dots, 2^j - 1$, define:

$$h_{j,k}(t) := 2^{j/2} \frac{1}{\sqrt{2}} \left(\mathbf{1}_{\left[-1 + \frac{2k}{2^j}, -1 + \frac{2(k+0.5)}{2^j}\right)} - \mathbf{1}_{\left[-1 + \frac{2(k+0.5)}{2^j}, -1 + \frac{2(k+1)}{2^j}\right)} \right).$$

The collection $\{h_0\} \cup \{h_{j,k}\}_{j,k}$ forms a complete orthonormal system for $L^2(-1, 1)$.

G. Further Analysis on Semi-dual Optimal Transport

G.1. Ill-posedness and Spurious Solutions in Non-regular Settings

As established in Proposition C.1, the regular assumption on the source measure $\mu \in \mathcal{P}_2^r(H)$ is a critical requirement for the well-posedness of the Monge map T^* . In practice, this theoretical guarantee serves as a prerequisite for the stable training of Neural OT models. Below, we present two examples demonstrating that **without the regular condition**, the SNOT objective becomes ill-posed, admitting **infinitely many spurious solutions** that fail to recover the true transport map.

To construct these examples, let $H = L^2((-1, 1))$ and consider the standard Fourier orthonormal basis $\{e_k\}_{k \in \mathbb{N}}$. We define two basis functions for distinct nonnegative integers k_1, k_2 :

$$e_{k_1}(t) := \sin(k_1 \pi t), \quad \text{and} \quad e_{k_2}(t) := \sin(k_2 \pi t). \quad (33)$$

Let X and Y be independent random variables following the uniform distribution $\text{Unif}(-1, 1)$. The detailed constructions are provided in Appendix G.2.

Example 1. Non-uniqueness of the Monge Map We first define two H -valued random variables:

$$\mathbf{X} := X e_{k_1}, \quad \mathbf{Y} := Y e_{k_2}.$$

Their probability laws $\mu_{\mathbf{X}}$ and $\mu_{\mathbf{Y}}$ are supported on orthogonal lines L_1 and L_2 . Clearly, $\mu_{\mathbf{X}}$ is not regular because it is concentrated on a finite-dimensional subspace L_1 , which is a Gaussian null set in the infinite-dimensional Hilbert space H (Figure 3).

Due to the orthogonality ($L_1 \perp L_2$), the quadratic cost function decouples, leading to a constant transport cost for *any* coupling $\pi \in \Pi(\mu_{\mathbf{X}}, \mu_{\mathbf{Y}})$. This triviality results in two critical issues:

1. **Non-uniqueness of T^* :** There exist infinitely many Monge maps T^* .

2. **Spurious solutions:** In the max-min objective (Eq. 1), there exist an optimal Kantorovich potential (e.g., $V^*(y) = \frac{1}{2} \|y\|_H^2$) under which the inner minimization problem for T_θ becomes *independent* of the map T . Consequently, *any* measurable map T becomes a solution to

$$\inf_{T: H \rightarrow H} \mathcal{L}(V^*, T) \quad (34)$$

regardless of whether it satisfies $T_\# \mu_{\mathbf{X}} = \mu_{\mathbf{Y}}$.

These observations highlight that the max-min formulation can allow infinitely many spurious solutions.

Example 2. Non-existence of the Monge Map In the second example, we consider a case where an optimal transport plan π^* exists (splitting mass), but no Monge map exists. Let R be a Rademacher random variable independent of X, Y . We define the random variables in H as:

$$\mathbf{X} := X e_{k_1}, \quad \tilde{\mathbf{Y}} := Y e_{k_1} + R e_{k_2}.$$

Here, the source measure $\mu_{\mathbf{X}}$ is supported on a single line segment, while the target $\mu_{\tilde{\mathbf{Y}}}$ is supported on two disjoint parallel segments (Figure 3).

We demonstrate that even if the optimal Kantorovich potential V^* is explicitly provided, the SNOT max-min formulation fails to recover a valid transport map. Specifically, the inner minimization problem for T_θ directs the map T to have zero horizontal displacement to minimize the transport cost. However, as shown in our analysis in Appendix G.2, any such map fails to satisfy the push-forward constraint because it cannot “split” the mass of $\mu_{\mathbf{X}}$ to cover the support of $\mu_{\tilde{\mathbf{Y}}}$. This identifies another spurious solution: for a given Kantorovich potential V^* , there is a solution T to inner minimization problem (Eq. 34), but T is not a valid Monge map, making it impossible for a neural network T_θ to learn the true coupling.

G.2. Details on Examples 1 and 2

G.2.1. EXAMPLE 1: PERPENDICULAR CASE

Setup. Let k_1 and k_2 be two distinct nonnegative integers. Define the basis functions $e_{k_1}(t) := \sin(k_1 \pi t)$ and $e_{k_2}(t) := \sin(k_2 \pi t)$. Let X and Y be real-valued random variables following the continuous uniform distribution $\text{Unif}(-1, 1)$. We

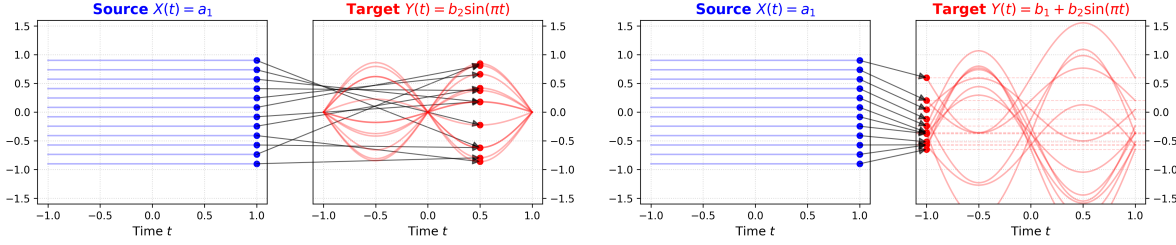


Figure 3. Illustration of optimal transport maps in Example 1

define two H -valued random variables:

$$\mathbf{X} := X e_{k_1}, \quad \mathbf{Y} := Y e_{k_2}.$$

Let $\mu_{\mathbf{X}}$ and $\mu_{\mathbf{Y}}$ denote the probability laws of \mathbf{X} and \mathbf{Y} in H , respectively. Their supports are given by the orthogonal lines:

$$L_1 := \{ae_{k_1} : a \in (-1, 1)\}, \quad L_2 := \{be_{k_2} : b \in (-1, 1)\}.$$

Note that $\mu_{\mathbf{X}}$ is not regular because it is concentrated on a finite-dimensional subspace L_1 , which is a Gaussian null set in the infinite-dimensional Hilbert space H .

Kantorovich's Problem. Consider the Kantorovich problem with quadratic cost between $\mu_{\mathbf{X}}$ and $\mu_{\mathbf{Y}}$:

$$\begin{aligned} C(\mu_{\mathbf{X}}, \mu_{\mathbf{Y}}) &:= \inf_{\pi \in \Pi(\mu_{\mathbf{X}}, \mu_{\mathbf{Y}})} \int_{H \times H} \frac{1}{2} \|x - y\|_H^2 \pi(dx, dy) \\ &= \inf_{\pi \in \Pi(\mu_{\mathbf{X}}, \mu_{\mathbf{Y}})} \int_{L_1 \times L_2} \frac{1}{2} \|x - y\|_H^2 \pi(dx, dy). \end{aligned} \quad (35)$$

Since the supports are orthogonal ($L_1 \perp L_2$), for any $x \in L_1$ and $y \in L_2$, the Pythagorean theorem implies $\|x - y\|_H^2 = \|x\|_H^2 + \|y\|_H^2$. Consequently, for any coupling $\pi \in \Pi(\mu_{\mathbf{X}}, \mu_{\mathbf{Y}})$, the total transport cost is constant:

$$\begin{aligned} \int_{L_1 \times L_2} \|x - y\|_H^2 \pi(dx, dy) &= \int_{L_1} \|x\|_H^2 \mu_{\mathbf{X}}(dx) + \int_{L_2} \|y\|_H^2 \mu_{\mathbf{Y}}(dy) \\ &= \mathbb{E} [\|\mathbf{X}\|_H^2 + \|\mathbf{Y}\|_H^2] = \frac{2}{3}. \end{aligned}$$

Since the cost is independent of the coupling π , every coupling is an optimal transport plan. This triviality implies a catastrophic loss of uniqueness for the Monge map. Specifically, let $\psi : (-1, 1) \rightarrow (-1, 1)$ be any measure-preserving map with respect to the uniform measure (e.g., $\psi(t) = t$, $\psi(t) = -t$, or any rearrangement). Then, the map $T_{\psi} : L_1 \rightarrow L_2$ defined by

$$T_{\psi}(ae_{k_1}) := \psi(a)e_{k_2}$$

is a valid Monge map pushing $\mu_{\mathbf{X}}$ forward to $\mu_{\mathbf{Y}}$. Since there are infinitely many such maps ψ , the optimal transport map is not unique.

Max-Min Problem and Spurious Solutions. We now show that this setting leads to spurious solutions in the max-min formulation. Let $V^*(y) := \frac{1}{2} \|y\|_H^2$. Since $V^* \in S_c$, the c -transform is explicitly calculated as:

$$(V^*)^c(x) := \inf_{y \in L_2} [c(x, y) - V^*(y)] = \inf_{y \in L_2} \left[\frac{1}{2} \|x\|_H^2 + \frac{1}{2} \|y\|_H^2 - \frac{1}{2} \|y\|_H^2 \right] = \frac{1}{2} \|x\|_H^2, \quad \forall x \in L_1.$$

Therefore, the dual objective value is:

$$\int_{L_1} (V^*)^c(x) \mu_{\mathbf{X}}(dx) + \int_{L_2} V^*(y) \mu_{\mathbf{Y}}(dy) = \frac{1}{6} + \frac{1}{6} = \frac{1}{3} = C(\mu_{\mathbf{X}}, \mu_{\mathbf{Y}}).$$

Thus, V^* is indeed an optimal Kantorovich potential.

Now, consider the inner minimization problem for this fixed potential V^* :

$$\inf_{T:L_1 \rightarrow L_2} \int_H (c(x, T(x)) - V^*(T(x))) \mu_{\mathbf{X}}(dx).$$

Using the orthogonality condition again, the integrand simplifies significantly:

$$c(x, T(x)) - V^*(T(x)) = \left(\frac{1}{2} \|x\|_H^2 + \frac{1}{2} \|T(x)\|_H^2 \right) - \frac{1}{2} \|T(x)\|_H^2 = \frac{1}{2} \|x\|_H^2.$$

Notice that the term depending on $T(x)$ has vanished perfectly. Therefore, the inner objective function is:

$$\inf_{T:L_1 \rightarrow L_2} \int_{L_1} (c(x, T(x)) - V^*(T(x))) \mu_{\mathbf{X}}(dx) = \int_{L_1} \frac{\|x\|_H^2}{2} \mu_{\mathbf{X}}(dx).$$

This implies that for the pair (V^*, T) , the global objective $\mathcal{L}(V^*, T)$ attains the primal cost $C(\mu_{\mathbf{X}}, \mu_{\mathbf{Y}})$ for **any** measurable function $T : L_1 \rightarrow L_2$. In other words, the objective function becomes completely independent of the choice of the map T . Consequently, even if the Kantorovich potential V^* is explicitly provided, the optimization problem fails to provide any gradient signal to guide T toward a valid Monge map. This demonstrates that attaining the optimal dual cost is insufficient for recovering the OT map in this singular setting, making the learning problem fundamentally ill-posed.

G.2.2. EXAMPLE 2: ONE-TO-MANY CASE.

Setup. Let R be a Rademacher random variable independent of $X, Y \sim \text{Unif}(-1, 1)$. We define the random variables in H as:

$$\mathbf{X} := X e_{k_1}, \quad \tilde{\mathbf{Y}} := Y e_{k_1} + R e_{k_2}.$$

The support of $\mu_{\tilde{\mathbf{Y}}}$ consists of two disjoint parallel line segments:

$$L_3 := \{ae_{k_1} + be_{k_2} : a \in (-1, 1), b \in \{-1, 1\}\}.$$

Kantorovich's Problem. We propose the candidate plan π^* which splits the mass equally:

$$\pi^*(dx, dy) := \frac{1}{2} \delta_{x+e_{k_2}}(dy) \mu_{\mathbf{X}}(dx) + \frac{1}{2} \delta_{x-e_{k_2}}(dy) \mu_{\mathbf{X}}(dx).$$

Marginal Verification: For the source, $\pi^*(A \times H) = \int_A 1 \mu_{\mathbf{X}}(dx) = \mu_{\mathbf{X}}(A)$. For the target, using the symmetry of Y and $\mu_{\mathbf{X}} = \mu_{\tilde{\mathbf{Y}}}$, for any Borel set B :

$$\begin{aligned} \mu_{\tilde{\mathbf{Y}}}(B) &= \frac{1}{2} \mathbb{P}(Ye_{k_1} + e_{k_2} \in B) + \frac{1}{2} \mathbb{P}(Ye_{k_1} - e_{k_2} \in B) \\ &= \int_H \left(\frac{1}{2} 1_B(x + e_{k_2}) + \frac{1}{2} 1_B(x - e_{k_2}) \right) \mu_{\mathbf{X}}(dx), \end{aligned}$$

which matches the marginal of π^* .

Cost and Optimality: The cost of π^* is purely vertical:

$$\begin{aligned} \frac{1}{2} \int_{H \times H} \|x - y\|_H^2 \pi^*(dx, dy) &= \frac{1}{4} \int_H \|x - (x + e_{k_2})\|_H^2 \mu_{\mathbf{X}}(dx) + \frac{1}{4} \int_H \|x - (x - e_{k_2})\|_H^2 \mu_{\mathbf{X}}(dx) \\ &= \int_H \left(\frac{1}{4} \| - e_{k_2} \|_H^2 + \frac{1}{4} \| e_{k_2} \|_H^2 \right) \mu_{\mathbf{X}}(dx) = \frac{1}{2} \int_H \mu_{\mathbf{X}}(dx) = \frac{1}{2}. \end{aligned}$$

Now, we verify that $1/2$ is the optimal cost. Since for any $(\phi, \psi) \in L^1(H, \mu_{\mathbf{X}}) \times L^1(H, \mu_{\tilde{\mathbf{Y}}})$ satisfying $\phi(x) + \psi(y) \leq c(x, y)$, for $\pi \in \Pi(\mu_{\mathbf{X}}, \mu_{\tilde{\mathbf{Y}}})$, we have

$$\int_{H \times H} c(x, y) \pi(dx, dy) \geq \int_H \phi(x) \mu_{\mathbf{X}}(dx) + \int_H \psi(y) \mu_{\tilde{\mathbf{Y}}}(dy).$$

Put $\bar{\phi}(x) := 0$, and $\bar{\psi}(y) := 1/2$. For $(x, y) = (ae_{k_1}, be_{k_1} \pm e_{k_2}) \in L_1 \times L_3$,

$$c(x, y) = \frac{1}{2}\|x - y\|_H^2 = \frac{1}{2}\|(a - b)e_{k_1} \pm e_{k_2}\|_H^2 = \frac{|a - b|^2}{2} + \frac{1}{2} \geq \frac{1}{2} = \bar{\phi}(x) + \bar{\psi}(y).$$

Therefore,

$$\frac{1}{2} = \int_{H \times H} c(x, y) \pi^*(dx, dy) \geq \inf_{\pi \in \Pi(\mu_{\mathbf{X}}, \mu_{\tilde{\mathbf{Y}}})} \int_{H \times H} c(x, y) \pi(dx, dy) \geq \int_H \phi(x) \mu_{\mathbf{X}}(dx) + \int_H \psi(y) \mu_{\tilde{\mathbf{Y}}}(dy) = \frac{1}{2}.$$

By the Kantorovich duality theorem (e.g. (Villani et al., 2009, Theorem 5.10)), $1/2$ is the optimal cost, and π^* is an OT plan.

Non-existence of Monge Map: We show that any Monge map $T : L_1 \rightarrow L_3$ yields a cost strictly larger than $1/2$. Since T must be a deterministic function, for each $\lambda \in (-1, 1)$, the image $T(\lambda e_{k_1})$ must lie on either the upper line segment $L_3^{up} := \{\lambda e_{k_1} + e_{k_2} : \lambda \in (-1, 1)\}$ or the lower line segment $L_3^{down} = \{\lambda e_{k_1} - e_{k_2} : \lambda \in (-1, 1)\}$. We can decompose the map as:

$$T(\lambda e_{k_1}) = T_1(\lambda) e_{k_1} + S(\lambda) e_{k_2},$$

where $T_1 : (-1, 1) \rightarrow (-1, 1)$ determines the horizontal position and $S : (-1, 1) \rightarrow \{1, -1\}$ determines the vertical selection. The total cost is decomposed into vertical and horizontal components:

$$\mathcal{C}(T) = \frac{1}{4} \int_{-1}^1 \|\lambda e_{k_1} - (T_1(\lambda) e_{k_1} + S(\lambda) e_{k_2})\|_H^2 d\lambda = \underbrace{\int_{-1}^1 \frac{1}{4} |\lambda - T_1(\lambda)|^2 d\lambda}_{\text{Horizontal Cost}} + \underbrace{\int_{-1}^1 \frac{1}{4} |S(\lambda)|^2 d\lambda}_{\text{Vertical Cost}} \geq \int_{-1}^1 \frac{1}{4} |S(\lambda)|^2 d\lambda$$

Since $S(\lambda) \in \{1, -1\}$, the vertical cost is fixed at $\frac{1}{2}$. Thus, for T to be optimal (optimal cost = $1/2$), the horizontal cost must be zero, which implies $T_1(\lambda) = \lambda$ almost everywhere.

However, this leads to a contradiction with the push-forward constraint $T_{\#} \mu_{\mathbf{X}} = \mu_{\tilde{\mathbf{Y}}}$. Consider the upper segment L_3^{up} and the set of points mapped to it, $A := \{\lambda e_{k_1} : S(\lambda) = 1\} \subseteq L_1$. The push-forward condition on L_3^{up} requires that for any subset $B \subset L_3^{up}$, the mass must match. Specifically, $\mu_{\tilde{\mathbf{Y}}}$ is uniform on L_3^{up} with total mass $1/2$. Since L_3^{up} corresponds to the interval $(-1, 1)$ of length 2, the density of $\mu_{\tilde{\mathbf{Y}}}$ on this line is $1/4$ with respect to the Lebesgue measure (length). In contrast, $\mu_{\mathbf{X}}$ is uniform on $(-1, 1)$ with density $1/2$. If $T_1(\lambda) = \lambda$, then T acts as a rigid translation on A . The measure of the image of A is:

$$\mu_{\tilde{\mathbf{Y}}}(T(A)) = \mu_{\tilde{\mathbf{Y}}}(\{\lambda e_{k_1} + e_{k_2} : S(\lambda) = 1\}) = \int_A \frac{1}{4} d\lambda = \frac{1}{4} \text{Length}(A).$$

On the other hand, the source measure is:

$$\mu_{\mathbf{X}}(A) = \int_A \frac{1}{2} d\lambda = \frac{1}{2} \text{Length}(A).$$

Due to the push-forward constraint, we require $\mu_{\mathbf{X}}(A) = \mu_{\tilde{\mathbf{Y}}}(T(A))$. This implies $\frac{1}{2} \text{Length}(A) = \frac{1}{4} \text{Length}(A)$, which is only possible if $\text{Length}(A) = 0$. However, to transport the total mass of $1/2$ to the upper segment, we must have $\mu_{\mathbf{X}}(A) = 1/2$, which requires $\text{Length}(A) = 1$. This contradiction implies that T_1 cannot be the identity map almost everywhere. Therefore, any valid transport map must involve horizontal displacement ($T_1(\lambda) \neq \lambda$), strictly increasing the cost:

$$\inf_T \mathcal{C}(T) > \frac{1}{2}.$$

This proves the non-existence of an optimal Monge map.

Max-Min Problem and Spurious Solutions. We now investigate the behavior of the max-min formulation under the Kantorovich potential. For any $y = \lambda e_{k_1} + \tilde{\lambda} e_{k_2} \in L_3$, we define the potential:

$$V^*(y) := \frac{1}{2}.$$

Since $V^* \in S_c$, the c -transform is explicitly calculated as follows. For any $x \in L_1$, let $x = ae_{k_1}$. Then:

$$(V^*)^c(x) := \inf_{y \in L_3} [c(x, y) - V^*(y)] = \inf_{b \in (-1, 1), \tilde{\lambda} \in \{-1, 1\}} \left[\left(\frac{1}{2} |a - b|^2 + \frac{1}{2} \right) - \frac{1}{2} \right] = \inf_{b \in (-1, 1)} \frac{1}{2} |a - b|^2 = 0.$$

The infimum is achieved when $b = a$. Therefore, the dual objective value is:

$$\int_{L_1} (V^*)^c(x) \mu_{\mathbf{X}}(dx) + \int_{L_3} V^*(y) \mu_{\mathbf{Y}}(dy) = 0 + \frac{1}{2} = C(\mu_{\mathbf{X}}, \mu_{\mathbf{Y}}).$$

Thus, V^* is indeed an optimal Kantorovich potential.

Now, consider the inner minimization problem for this fixed potential V^* :

$$\inf_{T: L_1 \rightarrow L_3} \int_H (c(x, T(x)) - V^*(T(x))) \mu_{\mathbf{X}}(dx).$$

Since $V^*(y) = 1/2$ for all $y \in L_3$, the term $V^*(T(x))$ is constant. For a map T decomposed as $T(\lambda e_{k_1}) = T_1(\lambda) e_{k_1} + S(\lambda) e_{k_2}$, the integrand becomes:

$$\begin{aligned} c(x, T(x)) - V^*(T(x)) &= \left(\frac{1}{2} |\lambda - T_1(\lambda)|^2 + \frac{1}{2} \right) - \frac{1}{2} \\ &= \frac{1}{2} |\lambda - T_1(\lambda)|^2. \end{aligned}$$

Since this term is non-negative, the infimum is clearly 0, achieved if and only if $T_1(\lambda) = \lambda$ almost everywhere. Therefore,

$$\inf_{T: L_1 \rightarrow L_3} \int_{L_1} (c(x, T(x)) - V^*(T(x))) \mu_{\mathbf{X}}(dx) = 0.$$

Combining this with the outer expectation, the global objective value is $0 + 1/2 = 1/2$, which matches the primal cost. The minimizers of the inner problem are of the form:

$$T(\lambda e_{k_1}) = \lambda e_{k_1} + S(\lambda) e_{k_2},$$

where $S(\lambda) \in \{1, -1\}$ is any measurable selection.

This leads to a contradiction. Mathematically, the pair (V^*, T) attains the optimal primal cost $C(\mu_{\mathbf{X}}, \mu_{\mathbf{Y}})$, making it a solution to the max-min problem. **However**, we explicitly proved that any map of this form (where $T_1(\lambda) = \lambda$) fails to satisfy the push-forward constraint $T_{\#} \mu_{\mathbf{X}} = \mu_{\mathbf{Y}}$ due to density mismatch (it requires a length expansion factor of 2, but the identity map has a factor of 1).

This implies that even when the true Kantorovich potential is provided, the max-min objective directs the generator T_{θ} toward a set of maps that are physically invalid. Consequently, the neural network cannot learn the optimal coupling π^* (which requires mass splitting) nor a valid approximation, proving that the formulation is ill-posed for learning Monge maps in this regime.

G.3. Revisiting Examples with Smoothing

We revisit the failure cases from Section G.1 to demonstrate how the proposed Gaussian smoothing strategy resolves the ill-posedness. Let $\gamma = \mathcal{N}(0, Q)$ be a non-degenerate centered Gaussian measure on H . The smoothed source $\mu_Q := \mu * \gamma$ belongs to $\mathcal{P}_2^r(H)$ by Theorem 4.3, ensuring the existence and uniqueness of the Monge map T_Q^* between μ_Q and the target ν .

Revisiting Example 1. In the original setting, the orthogonality of $\text{supp}(\mu_{\mathbf{X}})$ and $\text{supp}(\mu_{\mathbf{Y}})$ made the transport cost constant. This resulted in a "flat" optimization landscape where the objective $\mathcal{L}(V^*, \cdot)$ was minimized by any measurable map, leading to an infinite number of spurious solutions. By injecting Gaussian noise along the e_{k_2} -direction, we break this orthogonality and restore the geometric correlation between the source and target. This refinement ensures the functional $\mathcal{L}(V_Q^*, \cdot)$ has a unique minimizer (Theorem 3.2). Therefore, spurious solutions are eliminated, leaving only a single unique minimizer T_Q^* . See Figure 1.

Revisiting Example 2. In the original problem, the optimal transport plan requires splitting mass from a single point xe_{k_1} to two distinct target points $xe_{k_1} \pm e_{k_2}$. In this singular setting, a deterministic Monge map cannot exist, as a single-valued function is incapable of mapping one input to multiple disjoint outputs. Applying Gaussian smoothing regularizes the source to $\mu_Q \in \mathcal{P}_2^r(H)$, guaranteeing the existence of a unique Monge map T_Q^* (Proposition C.1). While the function T_Q^* cannot literally split a point, it approximates the splitting behavior by leveraging the continuous density of the smoothed support. Specifically, it maps local neighborhoods of x to different target segments (L_{up} and L_{down}). See Figure 1.

G.4. Saddle Points and Optimal Max-Min Solutions

Saddle Point. Following the consistency result established in Theorem 3.2 (2), this section provides a deeper analysis of the variational structure of the SNOT objective. Specifically, we clarify the rigorous relationship between **the saddle point**, **optimal max-min solutions**, and the identification of the **Kantorovich potential**.

We begin by formally defining the saddle point of the SNOT objective.

Definition G.1 (Saddle Point). A pair $(V^*, T^*) \in S_c \times \{T : H \rightarrow H\}$ is called a *saddle point* of the functional \mathcal{L} if it satisfies:

$$\sup_{V \in S_c} \mathcal{L}(V, T^*) \leq \mathcal{L}(V^*, T^*) \leq \inf_{T: H \rightarrow H} \mathcal{L}(V^*, T). \quad (36)$$

The existence of a saddle point is a stronger condition than the optimality of the max-min formulation. First, we establish that any saddle point is inherently an optimal max-min solution.

Proposition G.2 (Saddle Point implies Optimal Max-Min Solution). *If (V^*, T^*) is a saddle point, then it is an optimal max-min solution as defined in (Eq. 2) and (Eq. 3).*

Proof. The right inequality in (Eq. 36) implies that for all measurable maps T , $\mathcal{L}(V^*, T^*) \leq \mathcal{L}(V^*, T)$. Thus, T^* minimizes $\mathcal{L}(V^*, \cdot)$, satisfying (Eq. 3).

For the maximization part, let $h(V) := \inf_{T: H \rightarrow H} \mathcal{L}(V, T)$. For any $V \in S_c$, we have:

$$h(V) \leq \mathcal{L}(V, T^*).$$

From the left inequality in (Eq. 36), we know $\mathcal{L}(V, T^*) \leq \mathcal{L}(V^*, T^*)$. Combining these with the right inequality (which implies $\mathcal{L}(V^*, T^*) = h(V^*)$), we obtain:

$$h(V) \leq \mathcal{L}(V, T^*) \leq \mathcal{L}(V^*, T^*) = h(V^*).$$

Since $h(V) \leq h(V^*)$ for all V , V^* maximizes the inner minimization problem, satisfying (Eq. 2). Therefore, (V^*, T^*) is an optimal max-min solution. \square

However, the converse implication—whether an optimal max-min solution constitutes a saddle point—does not hold in general. This discrepancy is precisely where the issue of **spurious solutions** arises. While the set of optimal max-min solutions contains the true solution, it also includes numerous spurious pairs that fail to capture the optimal transport geometry.

To understand this, consider the case where T^* is a valid transport map (i.e., $T^* \# \mu = \nu$). In this scenario, for **any** measurable function V , the potential terms cancel out due to the change of variables formula:

$$\int_H V(y) \nu(dy) - \int_H V(T^*(x)) \mu(dx) = 0.$$

Consequently, the objective function becomes constant with respect to V :

$$\mathcal{L}(V, T^*) = \int_H c(x, T^*(x)) \mu(dx) = \text{Constant}.$$

This implies that **every** potential $V \in S_c$ maximizes the functional $\mathcal{L}(\cdot, T^*)$ (satisfying the left inequality of the saddle point condition), regardless of whether V is a true Kantorovich potential or an arbitrary function. Therefore, relying solely on the max-min optimality allows for spurious potentials that have no geometric connection to the cost function.

Consequently, the saddle point condition imposes a crucial constraint that rules out these spurious solutions. Specifically, the **inner minimization inequality** (the right inequality in (Eq. 36)) necessitates that T^* is the c -transform of V^* . This geometric link prevents V^* from being an arbitrary maximizer and ensures it qualifies as a valid Kantorovich potential. This observation leads to the following characterization.

Proposition G.3 (Characterization of Kantorovich Potential). *Let $\mu \in \mathcal{P}_2^r(H)$ and $\nu \in \mathcal{P}_2(H)$. Suppose that T^* is the Monge map and the pair (V^*, T^*) is a saddle point of \mathcal{L} . Then, V^* is a Kantorovich potential.*

Comparison with Finite-Dimensional Results. In the finite-dimensional Euclidean setting, recent work has demonstrated that the SNOT framework is free from spurious solutions provided the source measure assigns zero mass to sets with Hausdorff dimension at most $d - 1$ (Choi et al., 2025). This condition is slightly more general than our regular assumption (absolute continuity) in the finite-dimensional case, as discussed in Section 2. However, the validity of a direct infinite-dimensional analogue to this condition remains unclear due to the absence of the Lebesgue measure. While we conjecture that a similar geometric condition may hold in Hilbert spaces, pursuing this theoretical extension lies beyond the scope of our current study.

H. Implementation Details

H.1. Synthetic Data Experiments

In this section, we describe the experimental setup and the implementation details for the synthetic data experiments

Dataset Description Throughout this paragraph, let $e_1(t) := \sin(\pi t)$ and $e_2(t) := \sin(2\pi t)$ be the basis functions for $t \in [0, 1]$. We represent each signal as a linear combination of these bases, where $\mathbf{c} = (c_1, c_2) \in \mathbb{R}^2$ and $\mathbf{d} = (d_1, d_2) \in \mathbb{R}^2$ denote the coefficient vectors for the source signal $x(t) = \sum_{i=1}^2 c_i e_i(t)$ and the target signal $y(t) = \sum_{i=1}^2 d_i e_i(t)$, respectively. We consider the following four scenarios:

- **Perpendicular:** We generate the source coefficients $\mathbf{c} \sim \mu$ as follows: $c_1 \sim U([-1, 1])$ and $c_2 \equiv 0$. Similarly, we sample the target coefficients $\mathbf{d} \sim \nu$ by $d_1 \equiv 0$ and $d_2 \sim U([-1, 1])$.
- **Horizontal:** We generate $\mathbf{c} \sim \mu$ as follows: $c_1 \sim U([-1, 1])$, and $c_2 \equiv 0$. Similarly, we sample $\mathbf{d} \sim \nu$ by $d_1 \sim U([-1, 1])$ and $d_2 \equiv 0.5$.
- **One-to-Many:** We generate $\mathbf{c} \sim \mu$ as follows: $c_1 \sim U([-1, 1])$, and $c_2 \equiv 0$. Similarly, we sample $\mathbf{d} \sim \nu$ by $d_1 \sim U([-1, 1])$ and $d_2 \sim \text{Cat}(\{-0.5, 0.5\}, (0.5, 0.5))$.
- **Multi-Perpendicular:** Let $\mathbb{P} := \text{Cat}(\{-0.75, -0.25, 0.25, 0.75\}, (0.25, 0.25, 0.25, 0.25))$. We generate $\mathbf{c} \sim \mu$ by sampling $c_1 \sim U([-1, 1])$, and $c_2 \sim \mathbb{P}$. Similarly, we sample $\mathbf{d} \sim \nu$ by $d_1 \sim \mathbb{P}$ and $d_2 \sim U([-1, 1])$.

Training Details Across all experiments, we use the same network architecture and training hyperparameters unless otherwise stated. Both the potential function V_ϕ and the transport map T_θ are parameterized by neural networks composed of two Fourier layers (Li et al., 2020). In particular, the potential network V_ϕ additionally includes a final linear integral functional layer (Rahman et al., 2022). We train the models with a batch size of 256 for 5000 epochs. We set the OT cost parameter to $\tau = 0.2$ for the Multi-Perpendicular case, and $\tau = 0.001$ for all other cases. To improve the optimization of the inner-loop in the dual formulation of equation 11, we perform $K_T = 5$ updates of T_θ for every single update of v_ϕ . Regarding the regularization, we set $\lambda = 0$ for the Orthogonal case and $\lambda = 0.01$ otherwise.

For our experiments, we generate perturbed inputs $\hat{x}(t)$ as follows: $\hat{x}(t) = x(t) + \sigma \varepsilon(t)$, where $x(t)$ is a clean source signal and ε is a Fourier-basis noise. Specifically, we construct ε by expanding it on a Fourier basis $\{\epsilon_k(t)\}_{k \geq 1}$:

$$\varepsilon(t) = \sum_{k=1}^K \sqrt{\lambda_k} \xi_k \epsilon_k(t), \quad \xi_k \stackrel{\text{i.i.d.}}{\sim} \mathcal{N}(0, 1), \quad \lambda_k = \frac{1}{k^2}, \quad (37)$$

where we use $K = 16$ Fourier modes in all experiments. We employ a linear noise schedule from the initial noise $\sigma_{\max} = 0.5$ to the terminal noise $\sigma_{\min} = 0.06$. The noise level is updated over the first 80% of training epochs and kept fixed afterwards. At epoch e , the noise level is

$$\sigma = \max(\sigma_{\min}, (1 - t_e) \sigma_{\max} + t_e \sigma_{\min}), \quad t_e = \frac{e}{0.8E}, \quad \sigma_{\max} = 0.5, \quad \sigma_{\min} = 0.06, \quad (38)$$

where E is the total number of epochs.

H.2. Time Series Imputation

In this section, we describe the experimental setup and implementation details for the time series imputation task. We conduct experiments on ETTm1, ETTm2, ETTh1, ETTh2, and Exchange datasets (Wu et al., 2021). For each dataset, we

consider missing ratios of 0.5 and 0.7, and generate missing patterns following the same setup as [Wang et al. \(2025\)](#), and split the data into training, validation, and test sets with a ratio of 7:1:2.

Both the potential function V_ϕ and the transport map T_θ are parameterized using the Neural Fourier Model (NFM) ([Kim et al., 2024](#)). Unless otherwise specified, we follow [Kim et al. \(2024\)](#). We additionally adopt channel-independent modeling as in NFM and use a batch size of 1792. We train the model for 40 epochs with learning rate 2×10^{-4} , dropout 0.1, regularization weight $\lambda = 0.01$, and $\tau = 50$.

We follow the same input perturbation scheme as in the synthetic time-series experiments [H.1](#). We employ a linear noise schedule from the initial noise $\sigma_{\max} = 0.2$ to the terminal noise $\sigma_{\min} = 0.01$. The noise level is updated over the first 80% of the maximum schedule iterations and kept fixed afterwards:

$$\sigma_i = \max\left(\sigma_{\min}, \sigma_{\max} \left(1 - \frac{i}{0.8I}\right)\right), \quad \sigma_{\max} = 0.2, \sigma_{\min} = 0.01. \quad (39)$$

where i is the iteration index and I denotes the maximum schedule iterations. After $i \geq 0.8I$, the noise level stays at σ_{\min} .

Table 3. Comparison of Time-Series Imputation Performance for Missing Ratios 0.5 and 0.7. All baseline results (except Ours) are taken from Wang et al. (2025).

| Datasets | | ETTh1 | | ETTh2 | | ETTm1 | | ETTm2 | | Exchange | |
|--------------|-------|--------------|--------------|--------------|--------------|--------------|--------------|--------------|--------------|--------------|--------------|
| Methods | Ratio | MSE | MAE |
| Transformer | 0.5 | 0.249 | 0.359 | 0.250 | 0.360 | 0.069 | 0.173 | 0.032 | 0.122 | 0.261 | 0.215 |
| | 0.7 | 0.426 | 0.461 | 0.313 | 0.405 | 0.100 | 0.219 | 0.080 | 0.199 | 0.378 | 0.362 |
| DLinear | 0.5 | 0.148 | 0.272 | 0.117 | 0.240 | 0.110 | 0.229 | 0.089 | 0.206 | 0.252 | 0.208 |
| | 0.7 | 0.225 | 0.341 | 0.159 | 0.283 | 0.152 | 0.270 | 0.125 | 0.248 | 0.323 | 0.267 |
| TimesNet | 0.5 | 0.163 | 0.297 | 0.126 | 0.260 | 0.061 | 0.179 | 0.072 | 0.197 | 0.343 | 0.283 |
| | 0.7 | 0.523 | 0.532 | 0.168 | 0.295 | 0.110 | 0.238 | 0.114 | 0.243 | 0.401 | 0.332 |
| FreTS | 0.5 | 0.229 | 0.358 | 0.141 | 0.261 | 0.048 | 0.149 | 0.037 | 0.134 | 0.256 | 0.211 |
| | 0.7 | 0.236 | 0.351 | 0.176 | 0.294 | 0.074 | 0.187 | 0.042 | 0.137 | 0.201 | 0.166 |
| PatchTST | 0.5 | 0.153 | 0.284 | 0.137 | 0.269 | 0.046 | 0.139 | 0.029 | 0.116 | 0.204 | 0.169 |
| | 0.7 | 0.278 | 0.392 | 0.150 | 0.275 | 0.064 | 0.166 | 0.036 | 0.127 | 0.250 | 0.206 |
| SCINet | 0.5 | 0.169 | 0.300 | 0.176 | 0.285 | 0.062 | 0.173 | 0.077 | 0.206 | 0.280 | 0.231 |
| | 0.7 | 0.220 | 0.341 | 0.168 | 0.290 | 0.113 | 0.234 | 0.093 | 0.216 | 0.371 | 0.307 |
| iTransformer | 0.5 | 0.168 | 0.289 | 0.095 | 0.210 | 0.054 | 0.154 | 0.029 | 0.117 | 0.058 | 0.045 |
| | 0.7 | 0.244 | 0.353 | 0.155 | 0.263 | 0.082 | 0.191 | 0.057 | 0.167 | 0.116 | 0.095 |
| SAITS | 0.5 | 0.229 | 0.321 | 0.184 | 0.264 | 0.064 | 0.169 | 0.057 | 0.156 | 1.007 | 0.831 |
| | 0.7 | 0.343 | 0.395 | 0.287 | 0.341 | 0.094 | 0.207 | 0.061 | 0.164 | 1.006 | 0.833 |
| CSDI | 0.5 | 0.161 | 0.293 | 0.096 | 0.269 | 0.059 | 0.139 | 0.186 | 0.126 | 0.125 | 0.139 |
| | 0.7 | 0.213 | 0.312 | 0.117 | 0.273 | 0.252 | 0.273 | 0.136 | 0.174 | 0.143 | 0.161 |
| Sinkhorn | 0.5 | 0.910 | 0.669 | 0.820 | 0.614 | 0.950 | 0.708 | 0.905 | 0.678 | 0.740 | 0.611 |
| | 0.7 | 0.962 | 0.701 | 0.934 | 0.673 | 0.979 | 0.725 | 0.948 | 0.725 | 0.826 | 0.684 |
| TDM | 0.5 | 0.993 | 0.749 | 0.978 | 0.738 | 1.002 | 0.754 | 0.995 | 0.746 | 0.957 | 0.790 |
| | 0.7 | 0.989 | 0.749 | 1.017 | 0.751 | 1.004 | 0.757 | 1.001 | 0.749 | 0.981 | 0.812 |
| PWS-I | 0.5 | 0.125 | 0.234 | 0.047 | 0.145 | 0.048 | 0.133 | 0.021 | 0.096 | 0.032 | 0.026 |
| | 0.7 | 0.194 | 0.289 | 0.059 | 0.165 | 0.066 | 0.158 | 0.029 | 0.110 | 0.039 | 0.033 |
| Ours | 0.5 | 0.157 | 0.252 | 0.043 | 0.134 | 0.055 | 0.136 | 0.018 | 0.081 | 0.003 | 0.040 |
| | 0.7 | 0.272 | 0.323 | 0.052 | 0.153 | 0.076 | 0.163 | 0.023 | 0.096 | 0.005 | 0.043 |